Mon. Not. R. astr. Soc. (1980) **190**, 903–924 and *Microfiche* MN 190/2

The relation between radio luminosity and spectrum for extended extragalactic radio sources

R. A. Laing and J. A. Peacock *Mullard Radio Astronomy Observatory, Cavendish Laboratory, Madingley Road, Cambridge CB3 0HE*

Received 1979 July 31; in original form 1979 July 6

Summary. We have investigated the relation between radio spectrum and radio luminosity for samples of extragalactic radio sources selected at 178 and 2700 MHz. Spectra were derived for the extended regions of emission in these sources, which we have also classified by morphological type. At low frequencies the degree of spectral curvature is found to be correlated with luminosity for sources with hot-spots. The spectra of powerful sources show downward curvature which is greatest for the most luminous objects, whereas weak sources have spectra which steepen at low frequencies.

At high frequencies, the correlation between spectral index and luminosity is confirmed and is shown to extend throughout the luminosity range considered. This relation is due mainly to sources with hot-spots and implies an even stronger relation for the hot-spots themselves.

1 Introduction

The existence of a correlation between luminosity and spectral index for extragalactic radio sources, in the sense that spectra steepen with increasing radio luminosity, was first suggested by Heeschen (1960). More recent discussions were given by Macleod & Doherty (1972), Bridle, Kesteven & Guindon (1972) and Véron, Véron & Witzel (1972). These authors conclude that the correlation holds primarily for radio galaxies with straight spectra, although quasars continue the relation to higher luminosities.

It is now possible to improve on the earlier work in the following ways:

(1) Complete samples of extragalactic radio sources can be selected at both low and high frequencies.

(2) Many more optical identifications and redshifts are available, so that distant galaxies are not discriminated against.

(3) High-resolution radio observations have been made of all the sources considered in this paper, so that:

(a) Sources which are dominated by a compact (< 100 pc) component coincident with the optical identification can be recognized and discarded. Such objects have very high brightness temperatures and their spectra are affected by synchrotron self-absorption over the entire observable frequency range. The energy distribution of the radiating electrons is therefore not related to the spectrum.

(b) Compact *central* components in extended sources also have self-absorbed spectra but are identifiable on synthesis maps so that their flux densities can be subtracted. The spectrum of large-scale (> 1 kpc) emission, unbiased by the presence of central components, can therefore be derived for all extended sources.

(c) Morphological classification of extended sources is now possible. In particular, the spectral characteristics of sources with hot-spots can be studied separately from those of complex, low-luminosity objects.

(4) The presence of spectral curvature can provide valuable information about physical conditions in a source. This can now be investigated systematically for *extended* emission alone, without the biasing effects of central components.

The two mechanisms which are most likely to produce curvature in the spectrum of radiation from an electron energy distribution initially of power-law form are (e.g. Pacholczyk 1970):

(a) energy losses by synchrotron radiation, which cause downward curvature at high frequencies, and

(b) self-absorption of radiation from regions of high brightness temperature.

We have selected statistically complete samples at 178 MHz and at 2700 MHz (Section 2.1). The morphological classification of the sources is discussed in Section 2.2. We have compiled a set of flux densities over the range 10–14 900 MHz (Section 3.1), adjusted to the scale of Baars *et al.* (1977). All these sources have been observed with the Cambridge 5-km telescope at either 2.7 or 5.0 GHz. The spectra of the extended regions have been derived by subtraction of the flux densities from compact central components (Section 3.2). In Section 4 we investigate the variation of spectral *curvature* with luminosity, and in Section 5 the variation of spectral *index* with luminosity for the different morphological types together with the relations between α, redshift and compactness. Section 6 contains a brief discussion and a summary of the main conclusions.

2 The source samples

2.1 SELECTION CRITERIA

In order to reduce selection effects, we have used two complete samples of extragalactic radio sources defined at 178 MHz and at 2700 MHz by the following criteria:

178 MHz

(a) $S_{178} \geqslant 10$ Jy on the KPW scale (Kellermann, Pauliny-Toth & Williams 1969).

(b) $\delta \geqslant 10°$.

(c) $|b| \geqslant 10°$.

This is the sample listed by Jenkins, Pooley & Riley (1977) with the addition of 3C 296 (Birkinshaw, Laing & Peacock, in preparation) which was omitted from the original compilation because its declination is quoted incorrectly in the 3CR Catalogue (Bennett 1962). The original 3C survey was insensitive to sources of large angular size, and three such objects with $S_{178} \geqslant 10$ Jy have been discovered subsequently. These sources (DA 240, NGC 6251 and 4C 73.08) should be included in the sample, but have not been considered in this paper because their integrated flux densities are not well known. The same is true for 3C 236 and 3C 326, which have also been omitted. 165 sources remain.

Table 1. Identification contents for the two samples.

	178 MHz		2700 MHz	
	number	per cent	number	per cent
Extended sources				
Quasars	24	15	11	7
Galaxies with measured redshifts	71	43	52	32
Galaxies with estimated redshifts	27	16	11	7
Unidentified	16	10	4	2
All extended sources	138	84	78	48
Compact sources	27	17	83	52
Total	165	100	161	100

2700 MHz

(a) $S_{2700} \geqslant 1.5$ Jy on the KPW scale.
(b) $70° \geqslant \delta \geqslant 10°$.
(c) $|b| \geqslant 10°$.

This sample has been compiled by Peacock & Wall (in preparation), who describe the selection procedure. It includes a large proportion of flat-spectrum, compact sources, which are not considered in this paper. Of the remainder, 72 are included in the 178-MHz sample, whereas seven are not.

The identification contents of the two samples are summarized in Table 1.

2.2 MORPHOLOGICAL CLASSIFICATION

The spectra of compact (< 100 pc) regions are dominated by synchrotron self-absorption throughout the observable frequency range. If we are interested in the distribution of electron energies in a source, we must ignore such emission and consider only radiation from extended regions. We therefore need to separate sources whose emission at the selection frequency is dominated by a compact component (CC) from those with structure on scales > 1 kpc.

The angular resolution of currently available synthesis maps is insufficient to distinguish between CC's and distant extended sources whose angular sizes are comparable with the beamwidth used. We have therefore classed as compact all sources whose angular size is less than 2 arcsec (i.e. those unresolved by the 5-km telescope at 5 GHz). This will include a few distant, extended sources, but any other selection criterion would have to be based on the source spectrum and would thus introduce undesirable selection effects. D2 sources (Miley 1971) with two components, one of which is coincident with the optical object, are also classed as compact.

We have further divided extended sources into three subsets: Classes I and II of Fanaroff & Riley (1974), FRI and FRII, and ambiguous classifications. In an FRI source, the ratio of the distance between the regions of highest surface brightness on opposite sides of the optical identification to the total extent of the source is less than 0.5, while for an FRII source the ratio is greater than 0.5. The purpose of this system is to discriminate between 'classical double' sources (e.g. Cyg A) which have conspicuous hot-spots at their outer edges, and the less luminous, more diffuse sources (e.g. the 3C31-type, bent-double and twin-tail sources of

Simon 1978). There are some sources which cannot be classified unambiguously under this scheme for one of the following reasons: the brightness peaks are of low contrast, so that the classification depends on resolution; the position of the optical identification is uncertain, or the available synthesis observations are inadequate. FRII sources can easily be identified from synthesis maps, but the classification of the remaining objects is subjective. They are listed in the Appendix (Table A1). The detailed description follows Simon (1978). 3C 231 (M82; a nearby Irr II galaxy) has been classified separately.

3 Flux densities, spectra and luminosities

3.1 FLUX DENSITY SCALES

Flux-density measurements are available between frequencies of 10 MHz and 14 900 MHz for most of the sources considered in this paper. To check that these are consistent with the best available absolute scale, we have adopted the spectra of Cas A and Cyg A given by Baars *et al.* (1977; BGPW) who fit empirical formulae to the absolute measurements. The fit is good for frequencies above 38 MHz but both spectra show severe downward curvature at lower frequencies. We have therefore used their fitted curves for $\nu \geqslant 38$ MHz and independent absolute measurements for $\nu < 38$ MHz. The uncertainties in calculated flux densities for Cas A and Cyg A are thought to be about 2 per cent between 300 and 30 000 MHz, rising to 5 per cent below 300 MHz. The adoption of these spectra entails corrections to commonly-used flux density scales which are listed in Table 2. We have used the correction factors given by BGPW for $\nu \geqslant 750$ MHz, but not at lower frequencies for the following reasons:

(a) The scales at 38 and 178 MHz are known to be non-linear so that correction factors based on the flux densities of Cas A or Cyg A will be incorrect. We have therefore used the scaling of Roger, Bridle & Costain (1973; RBC).

(b) BGPW do not quote correction factors for the scales at 86, 26.3, 22.25 and 10.03 MHz (references as in Table 2).

Further details are given in the notes to Table 2.

3.2 DERIVATION OF SPECTRAL INDICES

Compact central components make sizable contributions to the flux densities of some extended sources at high frequencies, so that the integrated spectra are incorrect representations of the emission from extended structure. By subtracting the contributions of CC's as determined from synthesis maps, we derived two spectra for such sources, for large-scale emission and for total flux density respectively.

The flux densities of central components were measured at frequencies ranging from 1.4 to 15.4 GHz (see Table A2 of the Appendix). These measurements are complete at 5 GHz for the 178-MHz sample, except for 3C 296. Fifty of the extended sources in this sample have detectable emission from a CC and, for these objects, flux densities at the standard frequencies were derived from the information referenced in Table A2. When measurements were available at two or more frequencies, the missing values and their errors were estimated by fitting a power law; when only one measurement was available, a flat spectrum was assumed, consistent with the average for CC's. The relatively large errors assigned to the CC flux densities in these cases reflect the uncertainties in this procedure, but there are only four sources in the 178-MHz sample for which this could

Table 2. Flux density measurements and scaling factors.

Frequency/ MHz	Reference for original measurement	Scaling factor	Reference for scaling factor
14900	Genzel, Pauliny-Toth, Preuss & Witzel (1976)	1.0	BGPW (see section 4.4)
10700	Kellermann & Pauliny-Toth (1973)	0.938	Based on S(Cyg A) = 140.8 Jy (BGPW) compared with 150 Jy (Kellermann & Pauliny-Toth); see section 4.
5000	Pauliny-Toth & Kellermann (1968) as in KPW	0.993	BGPW
2695	Kellermann, Pauliny-Toth & Tyler (1968) as in KPW	1.011	BGPW
1400	Bridle, Davis, Fomalont & Lequeux (1972) Pauliny-Toth, Wade & Heeschen (1966) as revised by KPW. New polarization corrections have been made	1.029	BGPW
750	Pauliny-Toth, Wade & Heeschen (1966) as revised by KPW	1.046	BGPW
178	KPW	1.09	RBC
86	Artyukh <u>et al</u>. (1969)	1.0	Based on S(Cyg A) = 16118 Jy and S(Cas A) = 20100 Jy (epoch 1969.5) at 81.5 MHz from BGPW. The measurements of Scott & Shakeshaft (1971) have been used to relate the 86 MHz scale to these values. The derived correction is 1.01±0.02
38	KPW	1.18	RBC
26.3	Viner & Erickson (1975)	1.0	Absolute measurements by Viner (1975)
22.25	Roger, Costain & Lacey (1969) RBC	1.15 1.0	RBC Absolute measurements by Roger, Costain & Lacey (1969)
10.03	Bridle & Purton (1968 RBC	1.20 1.0	RBC Absolute measurements by Bridle (1967)

introduce a significant change in the spectral index. A similar procedure has been adopted for the sources selected at 2700 MHz. No corrections were made at frequencies below 1400 MHz, where the CC's are very weak compared with the extended emission. Corrections at 1400 MHz are in general very small.

Despite the removal of contributions from CC's, a single power-law fits very few of the resulting spectra over the entire frequency range. This means that the approach of Bridle *et al.* (1972) and of Macleod & Doherty (1972), which restricts the analysis to sources with straight spectra, must be reassessed because such sources are unrepresentative.

Low-frequency curvature, which may be of either sign, is often highly significant at frequencies below 200 MHz. This must be a real effect, firstly because its magnitude is often much larger than any possible errors in the flux-density scales, and secondly because such errors would always give deviations in the same sense. Once the effects of CC's have been removed, curvature at frequencies above 5000 MHz is less severe than at low frequencies and is always in the downward sense (see Section 4.3). At intermediate frequencies, however, the spectra appear to be relatively straight and we have evaluated spectral indices α, defined in the sense that $S \propto \nu^{-\alpha}$, by fitting power laws to the flux densities measured at 750, 1400, 2695 and 5000 MHz, scaled as in Table 2. CC flux densities are relatively smaller and better determined over this range than they are at higher frequencies. Inaccuracies in the spectra of extended structure are small, and the fits to power laws are generally good.

The flux densities (in Jy), spectral indices and luminosities (in $\mathrm{W\,Hz^{-1}}$) for the 178-MHz sample (scaled as in Table 2) are listed on *Microfiche* MN 190/2.

3.3 LUMINOSITIES

Luminosities were evaluated at 1400 MHz both for the extended emission (using CC-subtracted flux densities and spectral indices) and for the total emission. This frequency was chosen because very accurate flux densities are available, and contributions from CC's are small. The redshifts for galaxies, when unknown, were estimated from a magnitude–redshift plot for radio galaxies. The assumed relation, and references for optical data, are listed in the Appendix (Table A3). A Hubble constant of $50\,\mathrm{km\,s^{-1}\,Mpc^{-1}}$ and a density parameter $\Omega_0 = 0$ have been assumed throughout.

4 The relation between spectral curvature and luminosity

4.1 INTRODUCTION

In order to test for spectral curvature, we have evaluated the ratio:

$$R = S_\nu / S_e$$

where S_ν is the flux density measured at frequency ν, and S_e is the flux density predicted from the power-law fit to the spectrum between 750 and 5000 MHz. Contributions from CC's have been subtracted. The analysis has been restricted to FRII sources for the following reasons:

(a) Many FRI sources have large angular sizes, so that few flux-density measurements have been attempted at high frequencies and the low-frequency values may be in error due to resolution effects (Table A1). Any estimates of spectral curvature would be incomplete and biased.

(b) The unclassified sources are of diverse physical types and some have very unusual spectra (see Section 4.4).

(c) The FRII sources are of limited angular extent and form a large, homogeneous class.

We have distinguished sources for which the values of R are likely to be seriously in error because of badly determined corrections for CC's or the effects of confusion.

4.2 SPECTRAL CURVATURE AT LOW FREQUENCIES

Fig. 1 a–f show plots of R against P_{1400} at frequencies below 750 MHz for all identified sources in the 178-MHz sample. The values of R are in general very different from 1, corresponding to deviations from straight spectra which are much larger than any possible errors in the flux densities. It is apparent that, for a given frequency in this range, R decreases with increasing luminosity. This result holds even if the flux-density scales are in error by constant factors.

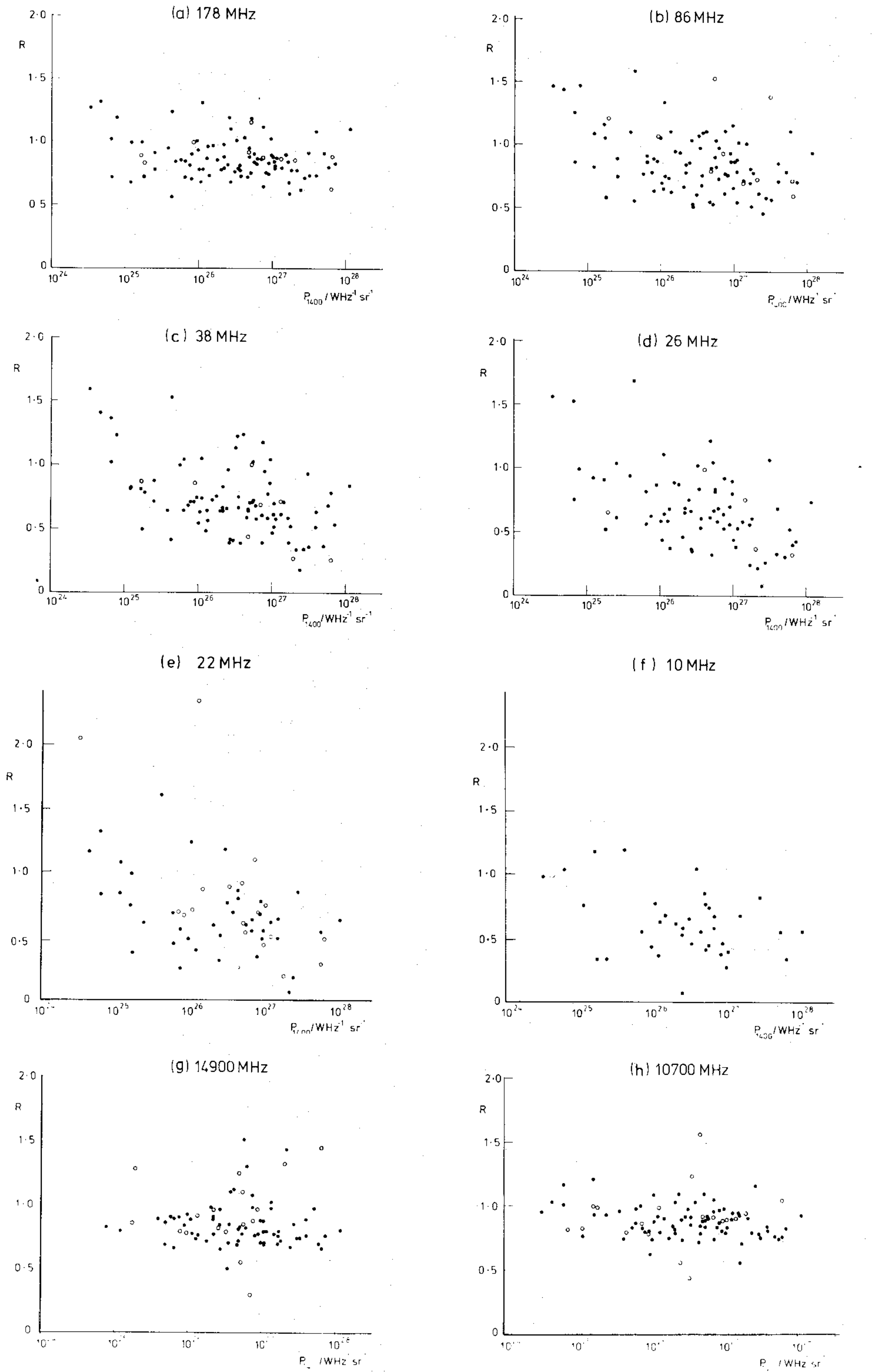

Figure 1. Plots of the ratio $R = S_\nu/S_e$ against luminosity for all identified FRII sources in the 178-MHz sample which have flux densities measured at the relevant frequencies. Open circles denote measurements which may be seriously in error (see Section 4.1).

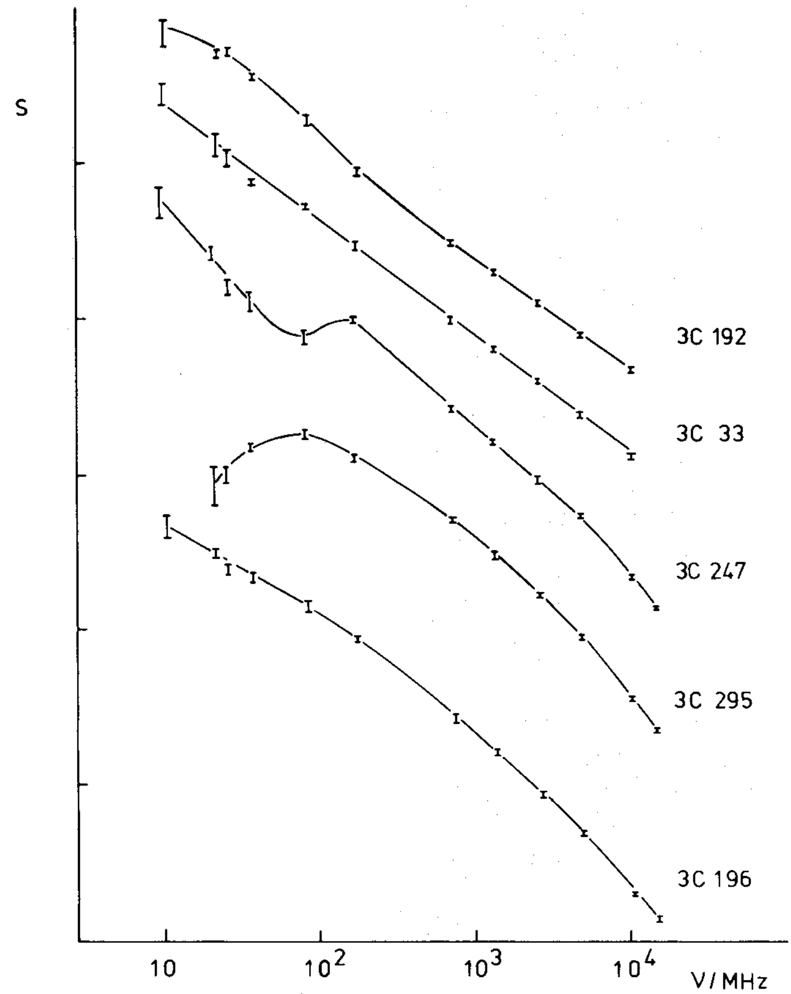

Figure 2. Examples of the spectra of extended sources. Flux density S (on an arbitrary scale) is plotted against frequency ν; both scales are logarithmic. The luminosities of the sources increase from top to bottom of the diagram.

The shapes of radio-source spectra are therefore correlated with their luminosities; some illustrative examples are shown in Fig. 2. The least-luminous sources ($P_{1400} < 10^{25}\,\mathrm{W\,Hz^{-1}\,sr^{-1}}$) have values of $R > 1$, implying that their spectra steepen at low frequencies. An example is 3C 192 ($P_{1400} = 6.5 \times 10^{24}\,\mathrm{W\,Hz^{-1}\,sr^{-1}}$). A necessary explanation is that a steep-spectrum ($\alpha \sim 1$) component is present, possibly as a result of synchrotron or Inverse-Compton losses acting on a remnant of earlier activity in the source. Somewhat more powerful sources (e.g. 3C 33) have spectra which are approximately straight over the entire frequency range ($R \sim 1$). The recognition of a low-frequency component depends on its spectral index and luminosity relative to those of the higher-frequency structure. It is therefore plausible that such components are only more prominent in weak sources because the higher-frequency structure has a flatter spectrum ($\alpha \sim 0.7$) and is relatively less luminous.

Apart from those for the least-luminous galaxies (discussed above), the values of R are typically less than 1 and decrease with increasing *luminosity*. The spectra of powerful sources are curved downwards, so that R decreases with decreasing *frequency*. The mean values of R are given in Table 3 for various power ranges. The shapes of the spectra of the unidentified sources are consistent with the assumption that they are galaxies at large redshifts ($z \sim 1$) and consequently of high luminosity. The most luminous objects have $R \sim 0.5$ at the lowest frequencies.

Table 3. Ratios of observed to predicted flux densities.

Frequency/MHz	$\log(P_{1400}/\mathrm{W\ Hz^{-1}\ sr^{-1}})$				
	24.5 - 25.5	25.5 - 26.5	26.5 - 27.5	27.5 - 28.5	Unidentified sources
178	0.95 ± 0.06	0.88 ± 0.03	0.85 ± 0.02	0.85 ± 0.05	0.80 ± 0.04
86	1.07 ± 0.08	0.85 ± 0.04	0.84 ± 0.03	0.78 ± 0.06	0.71 ± 0.05
38	0.99 ± 0.09	0.72 ± 0.04	0.69 ± 0.04	0.56 ± 0.07	0.53 ± 0.06
26.3	0.95 ± 0.11	0.71 ± 0.06	0.65 ± 0.05	0.47 ± 0.06	0.48 ± 0.06
22.25	1.00 ± 0.15	0.77 ± 0.13	0.61 ± 0.05	0.48 ± 0.07	0.39 ± 0.06
10.3	0.77 ± 0.15	0.58 ± 0.08	0.59 ± 0.05	0.48 ± 0.07	0.47 ± 0.16

To summarize: weak sources have spectra which steepen at low frequencies; powerful sources have spectra which flatten. The former effect can be attributed to the presence of extended components with steep spectra.

4.3 SPECTRAL CURVATURE AT HIGH FREQUENCIES

In Fig. 1(g) and (h) the ratios R at frequencies of 14 900 and 10 700 MHz are plotted as a function of luminosity for all the identified FRII sources in the 178-MHz sample which have flux densities measured at the relevant frequencies. These diagrams show the following features:

(a) R is independent of luminosity.

(b) Of the sources with $R > 1$, very few have accurate flux-density measurements, in particular because of uncertainties in the subtraction of CC's. Points which are very uncertain are indicated separately in Fig. 1(g) and (h).

(c) The mean values of R are significantly less than 1. For all FRII objects (including unidentified sources) with accurate subtraction of flux densities from CC's, the mean values are:

$\langle R_{14900} \rangle = 0.838 \pm 0.023$ (73 sources),

$\langle R_{10700} \rangle = 0.868 \pm 0.013$ (89 sources).

The spectra therefore seem to curve *downwards* at high frequencies.

At high frequencies, we can extrapolate only over a range of $\log \nu$ which is small compared with that available at low frequencies (Section 4.2). The values of R_{14900} and R_{10700} are therefore closer to 1 than are those at frequencies below 750 MHz and it is not obvious whether the curvature is real or is caused by errors in the flux-density scales at 10 700 and 14 900 MHz.

In order to clarify this problem, we have considered the following two alternatives:

(a) The flux-density scales are correct and the spectral curvatures are real. In this case, since the observed curvatures are relatively small, it should be possible to fit the spectra by parabolae $\log S = a + b \log \nu + c(\log \nu)^2$.

(b) All spectra are straight and the flux-density scales at 10 700 and at 14 900 MHz are in error by constant factors. The spectra should then become power laws when S_{14900} and S_{10700} are divided by the mean values of R given earlier.

We have tested both these assumptions for the 73 FRII sources whose spectra are well-determined between 750 and 14 900 MHz. The distributions of χ^2 which resulted from the fitting procedures were compared with the theoretical predictions by means of the Kolmogorov–Smirnov test. The observed and predicted distributions *are* consistent for parabolic fits (case a) but not for straight spectra with scaling errors (case b). The data are therefore fitted well by spectra which curve smoothly between 750 and 14 900 MHz.

In particular, we can identify those sources whose spectra show unambiguous evidence for intrinsic downward curvature at high frequencies. We have selected sources for which $R_{14900} < 0.8$ and whose spectra from 750 to 14 900 MHz, with the standard flux-density scales of Section 3, are significantly different from power laws (at the 1 per cent level, using the χ^2 test). This should ensure that the large values of χ^2 are due to consistent downward curvature rather than to random scatter in the measurements. The sources are listed in Table 4. It is interesting to note that all the sources are relatively luminous ($P_{1400} > 10^{26}$ W Hz^{-1} sr^{-1}).

4.4 MODELS FOR SPECTRAL CURVATURE

A natural explanation for the low-frequency curvature in luminous sources is that the hot-spots in FRII sources have turnover frequencies in the range 10–150 MHz due to synchrotron self-absorption. Readhead & Longair (1975) and Jenkins & McEllin (1977) have shown that the fraction of emission in such small-scale structure increases with increasing luminosity. The low-frequency curvature is therefore expected to be most severe for the very powerful

Table 4. FRII sources whose spectra show significant downward curvature at high frequencies.

Source (3C)	Identification	$\log(P_{1400}/\mathrm{W\,Hz^{-1}\,sr^{-1}})$
6.1	Galaxy	27.22
14	Galaxy	26.26*
19	Galaxy	26.56
41	Galaxy	26.91*
123	Galaxy	26.96
175.1	–	
184	Galaxy	27.51*
196	Quasar	27.86
205	Quasar	27.77
228	Galaxy	26.74*
247	Galaxy	26.44*
254	Quasar	27.06
268.1	–	
295	Galaxy	27.40
324	Galaxy	27.04*
325	Quasar ?	
330	Galaxy	27.03
336	Quasar	27.22
351	Quasar	26.35
441	Galaxy	26.98*
455	Quasar	26.66

* denotes that the redshift has been estimated

Table 5. Self-absorption turnover frequencies.

z	P_{1400}/W Hz^{-1} sr^{-1}	ν_{SSA}/MHz
0.03	1.6×10^{23}	16
0.1	1.9×10^{24}	24
0.3	2.0×10^{25}	34
1.0	3.9×10^{26}	97
3.0	9.6×10^{27}	140

sources, as observed. This is in agreement with the conclusions of van der Laan & Perola (1969) who found that sources with convex spectra are more likely to contain components of angular diameter < 1 arcsec than are those with straight spectra. The turnover frequencies due to synchrotron self-absorption in a typical hot-spot with a flux density of 0.5 Jy at 1400 MHz, $\alpha = 1$ at high frequencies and a linear size of 1 kpc, are given in Table 5 for a range of redshifts. A cubical source and equipartition of the energies of magnetic field and relativistic particles are assumed, but the calculated turnover frequencies are insensitive both to geometry and to magnetic field strength. The synchrotron spectrum of a power-law energy distribution of electrons is curved downwards below the frequency ν_{SSA} at which the source becomes optically thick, and the spectral index approaches -2.5 at lower frequencies. The turnover frequencies given in Table 5 are in precisely the right range to explain the observed low-frequency curvature.

Three examples of spectra showing low-frequency curvature are given in Fig. 2. The spectrum of 3C 295 has a turnover at 70 MHz and indicates that an extended source *can* show self-absorption; that of 3C 247 has a kink at 150 MHz which is likely to be due to the self-absorption of a compact hot-spot, and that of 3C 196 curves gradually below 100 MHz, probably due to a superposition of components with different sizes and turnover frequencies. In all cases, the observed spectra are consistent with the high-frequency structures (Pooley & Henbest 1974; Jenkins *et al* 1977).

The standard explanation for curvature at high frequencies is in terms of synchrotron radiation losses (e.g. Pacholczyk 1970). We have isolated those FRII sources which show definite downward curvature (Table 4) but the range of frequency over which the curvature is observed is too small to justify fitting detailed models. In contrast, two sources in the 178-MHz sample (3C 310 and 3C 338) have spectra with gross curvature over the range from 10 to 10 700 MHz, which can be fitted accurately by assuming initially isotropic, power-law energy distributions of electrons with index -2.5 (corresponding to $\alpha = 0.75$). The spectra after radiation losses, assuming no replenishment of electrons during a time t, are given by Pacholczyk (1977). With equipartition magnetic fields from Jaffe & Perola (1974) and van Breugel (1979) we derive the following ages:

	3C 310	3C 338
ν_t/MHz	2500	1000
B/T	3×10^{-10}	1×10^{-9}
t/yr	1×10^{8}	3×10^{7}

where ν_t is the turnover frequency and B is the magnetic field. The integrated spectra of these sources suggest that no replenishment of radiating electrons has taken place in the extended regions for the last 10^7–10^8 yr. The radio structures of the two sources are similar, with brightness peaks of low contrast surrounded by diffuse emission. Other sources of this morphological type also have anomalously steep spectra (Section 5.2), possibly for the same reason.

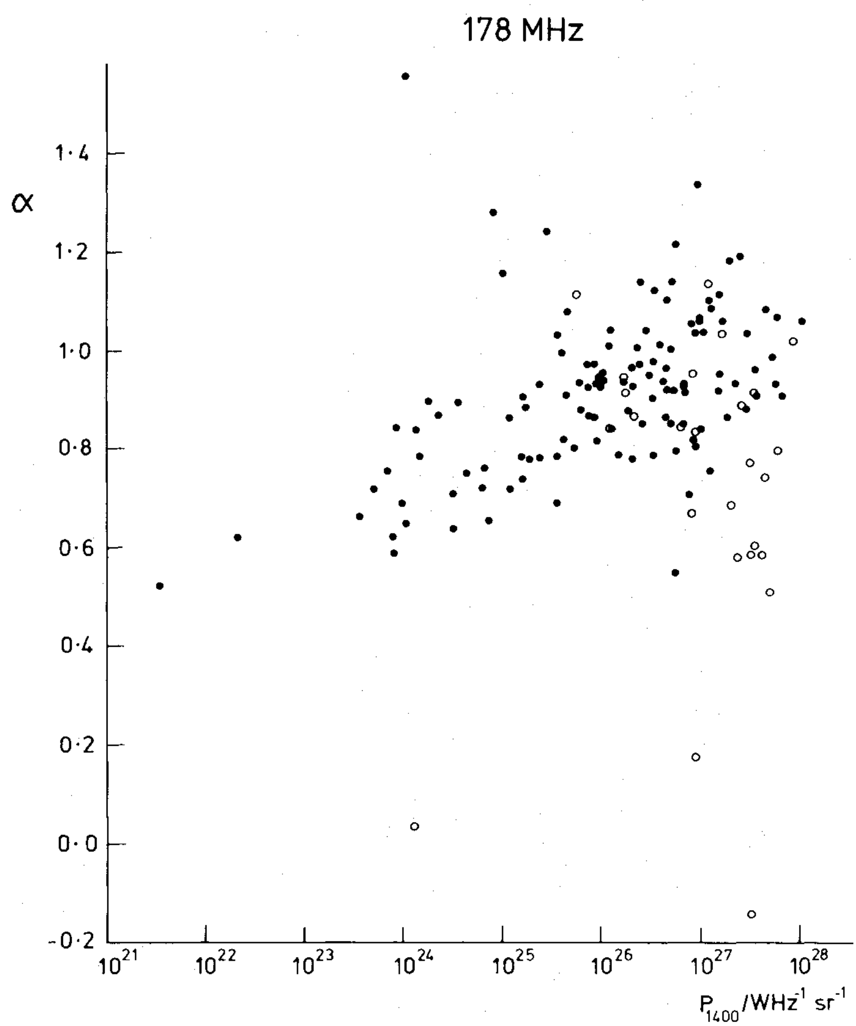

Figure 3. A plot of spectral index, α, against luminosity at 1400 MHz, P_{1400}, for all identified sources in the 178-MHz sample. Central components have *not* been subtracted. ● Extended sources; ○ compact sources.

5 The relation between spectral index and luminosity, redshift and compactness

5.1 THE P–α RELATION FOR COMPACT AND EXTENDED SOURCES

In Fig. 3 we have plotted against P_{1400} the spectral indices derived by fitting power laws to the spectra between 750 and 5000 MHz *before* central-component subtraction, for all the identified sources in the 178-MHz sample. Sources with emission dominated by CC's are distinguished from extended sources. With the exception of 3C 84 (a core-halo source associated with the active galaxy NGC 1275), all the compact objects have high luminosities ($P_{1400} > 10^{26}$ W Hz^{-1} sr^{-1}). Of these, about half lie in the region of the diagram occupied by the powerful extended sources and may therefore be unresolved double sources. The remainder of the compact objects have flatter spectra than do extended sources of comparable luminosity, and they form a separate class. As expected, the proportion of compact, flat-spectrum sources is much higher in the 2700-MHz sample (Table 1).

5.2 THE P–α RELATION FOR EXTENDED STRUCTURE

In the remainder of Section 5 we consider only extended emission, neglecting compact sources. 3C 231 (M82) has also been omitted since it is an atypical object of very low luminosity whose radio emission comes from a galactic disc, unlike that of any other object in the sample. All spectral indices and luminosities were calculated using flux densities from which contributions due to CC's had been subtracted.

We have plotted the distributions of these spectral indices for the two samples in Fig. 4, which reveals the following features:

(a) A deficit of sources with high spectral indices in the 2700-MHz sample, as expected.

(b) High spectral indices for the unidentified sources. Because of the correlation between luminosity and spectral index, as was noted by KPW, this is consistent with their being distant, powerful radio galaxies. The two unidentified sources with relatively flat spectra in the 2700-MHz sample lie in crowded optical fields, so that the correct identifications are uncertain.

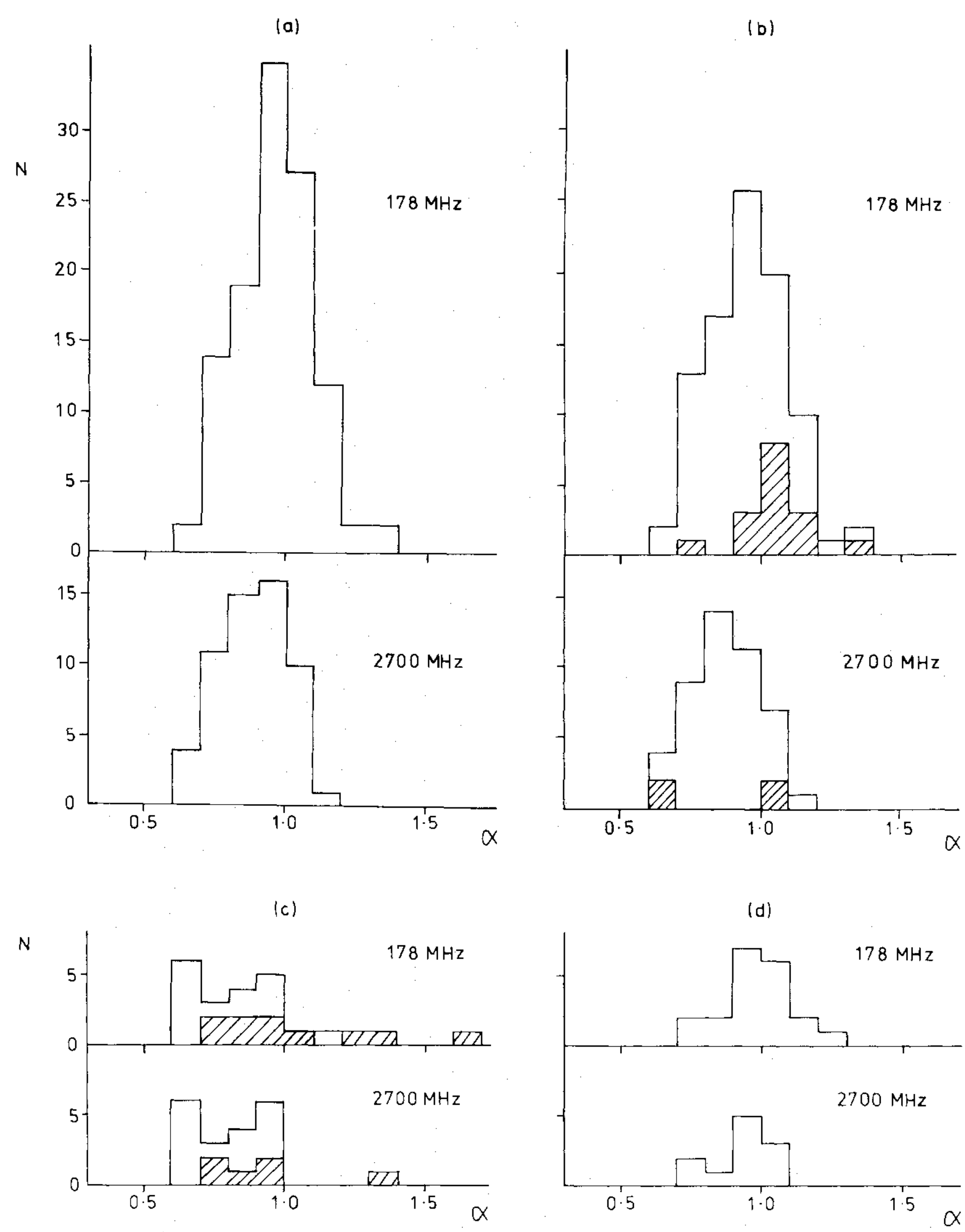

Figure 4. Spectral index distributions for extended sources in the two samples. Central components have been subtracted. (a) All FRII sources; (b) FRII galaxies and unidentified sources (hatched); (c) FRI and unclassified sources (hatched); (d) FRII quasars.

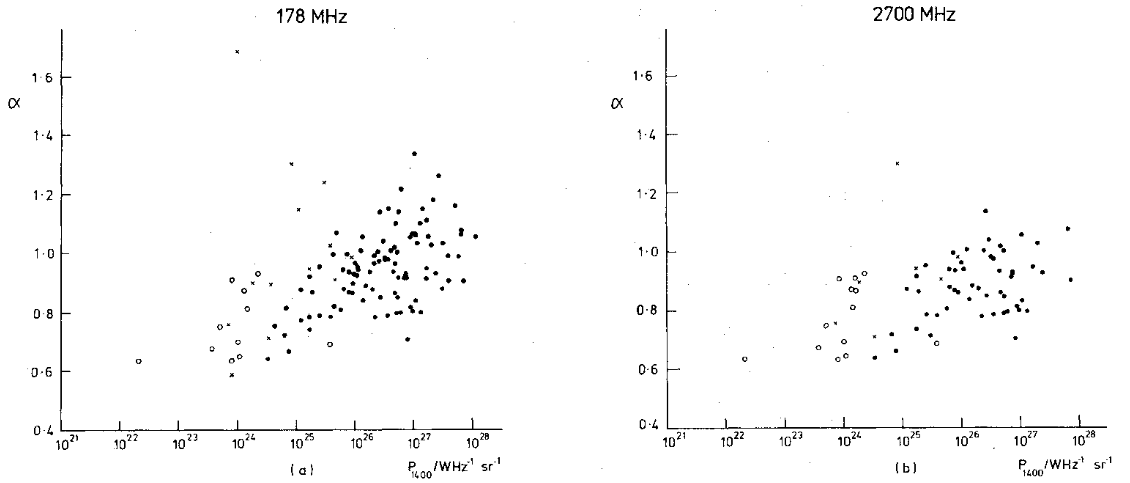

Figure 5. Plots of spectral index, α, against luminosity, P_{1400}, for extended sources. Central components have been subtracted. (a) 178-MHz sample; (b) 2700-MHz sample; ○ FRI; × unclassified; ● FRII.

(c) Fig. 4(c) shows that the FRI sources have relatively flat spectra, but the unclassified sources (a heterogeneous collection) have a wide range of spectral indices.

(d) The distribution of the spectral indices of extended emission in quasars (Fig. 4d) is consistent with that for the FRII galaxies.

Fig. 5 shows plots of α against P_{1400} for the extended sources, divided into the morphological classes of Section 2.2. There are strong correlations for both samples, significant at better than the 0.05 per cent level using the Spearman rank test. The correlation is due primarily to the FRII sources which are discussed in detail later (Section 5.3). The FRI sources continue the relation to lower luminosities. In particular, the 3C31-type sources (Simon 1978) have a mean spectral index of 0.74. This low value is probably due to the presence of jets with $\alpha \approx 0.5$ in such sources, and occurs despite large variations of spectral index across the sources (e.g. Burch 1977; Birkinshaw, Laing & Peacock, in preparation). Note that several such objects are of large angular size and the measured flux densities may suffer from resolution effects. The FRI sources show no correlation between α and P_{1400} when considered separately, but the range of luminosities is very small. The main difference between Fig. 5(a) and (b) lies in the absence of sources with steep spectra in the 2700-MHz sample, as expected from the higher selection frequency (see Section 5.1).

The unclassified sources include some objects with anomalously steep spectra (3C28, 310, 314.1, 319 and 338); these are discussed in more detail in Section 4.4.

5.3 THE P–α RELATION FOR FRII SOURCES

The bulk of the correlation between α and P_{1400} is due to the extended structure in FRII sources (Fig. 6), in particular those with $P_{1400} < 10^{26}$ W Hz^{-1} sr^{-1} (most such sources are common to both samples), but the scatter increases considerably at higher luminosities. The correlation is significant at the 0.05 and 1 per cent levels for the 178-MHz and 2700-MHz samples respectively. The fitted regressions lines of α on P_{1400} are:

$$\alpha = 0.088 \log (P_{1400}/\mathrm{W\,Hz^{-1}\,sr^{-1}}) - 1.38 \quad (178\ \mathrm{MHz}),$$

$$\alpha = 0.062 \log (P_{1400}/\mathrm{W\,Hz^{-1}\,sr^{-1}}) - 0.73 \quad (2700\ \mathrm{MHz}).$$

The quasars do not show a significant correlation when considered separately, but their distribution in the diagram overlaps that of the powerful galaxies. Errors in the estimation

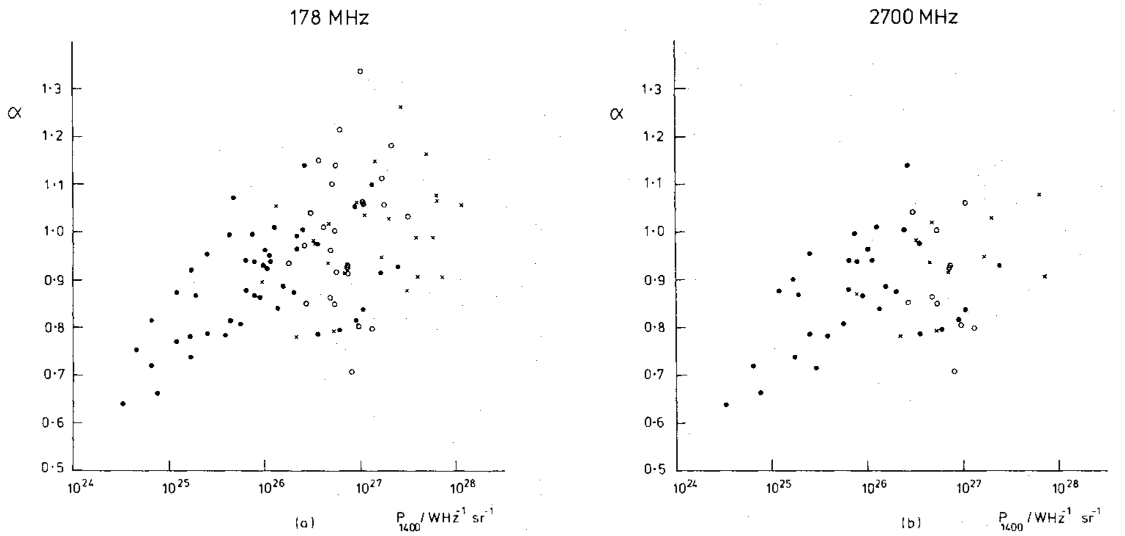

Figure 6. Plots of spectral index, α, against luminosity, P_{1400}, for FRII sources alone. Central components have been subtracted. (a) 178-MHz sample; (b) 2700-MHz sample; • galaxy with measured redshift; ○ galaxy with estimated redshift; × quasar.

of redshifts could change the detailed form of the diagram for $P_{1400} > 10^{26}\ \mathrm{W\,Hz^{-1}\,sr^{-1}}$, but cannot destroy the correlation. There are 16 unidentified sources in the 178-MHz sample which are expected to have $P_{1400} > 5 \times 10^{26}\ \mathrm{W\,Hz^{-1}\,sr^{-1}}$; these have relatively steep spectra (see Section 5.2) and follow the trend for powerful galaxies. There are only four unidentified extended sources in the 2700-MHz sample.

5.4 COMPARISON WITH PREVIOUS RESULTS

Of the previous analyses, our approach is closest to that of Véron *et al.* (1972) in that we selected sources on the basis of their morphologies. Radio maps of much higher resolution are now available, together with many more identifications and redshifts, so that a better morphological classification can be used for a larger example. Véron *et al.* considered 'elliptical radiogalaxies' (principally the low-power sources) selected at 178 MHz. This corresponds to the restriction that $P_{1400} < 10^{26}\ \mathrm{W\,Hz^{-1}\,sr^{-1}}$, the range over which the correlation is best defined. The slope of their regression line is 0.08, in good agreement with our value of 0.087 for the FRII sources in the 178-MHz sample.

Bridle *et al.* (1972) considered sources selected at 1400 MHz whose spectra appeared to be straight between 100 and 7000 MHz, including some FRI sources and a few powerful FRII sources. Their regression line has a slope of ≈ 0.06, close to our slope for the 2700-MHz sample, as expected.

Macleod & Doherty (1972) suggested that the correlation was entirely due to galaxies with straight spectra. Since they considered spectra defined between 10 MHz and 10 700 MHz, their sample was restricted to low luminosities (see Section 4.2). In this region, the correlation for the FRII sources is much steeper than over our entire luminosity range (see Fig. 6) and this may explain the high slope of 0.21 for their regression line.

5.5 SPECTRAL INDEX AND REDSHIFT FOR FRII SOURCES

Plots of spectral index against redshift (Fig. 7a and b) are very similar to the corresponding plots of α against P_{1400}. This is as expected, since luminosity and redshift are very strongly

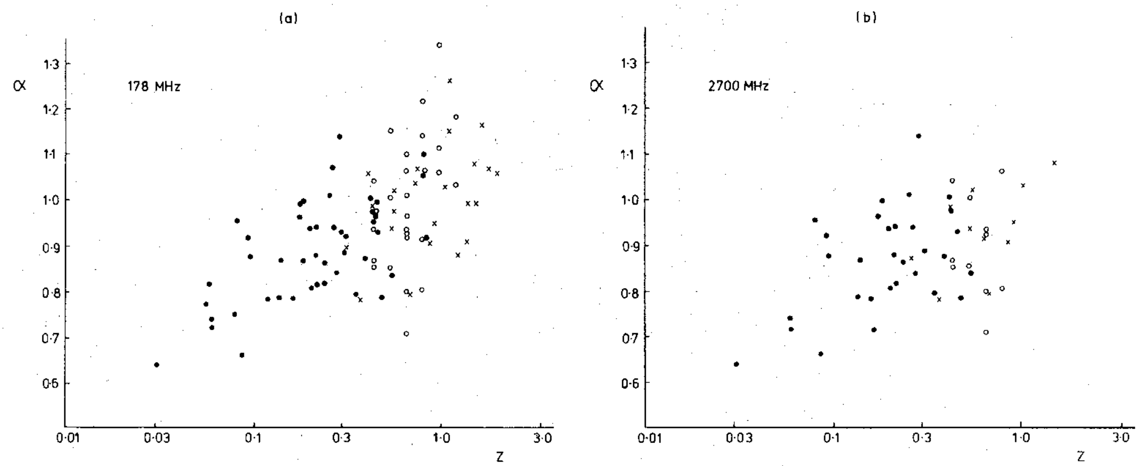

Figure 7. Plots of spectral index, α, against redshift, z, for FRII sources. Central components have been subtracted. (a) 178-MHz sample, (b) 2700-MHz sample. ● Galaxy with measured redshift; ○ galaxy with estimated redshift; × quasar.

correlated for samples selected to have flux densities above such relatively high limits. It is therefore impossible to say whether α depends primarily on luminosity or on redshift. Indirect evidence that the luminosity effect is the fundamental one comes from the work of Meier *et al.* (1979) and Katgert, de Ruiter & van der Laan (1979). They suggest that the properties of the radio-source population show little evolution for $z < 0.25$ and this is the range over which the correlation is best defined.

5.6 SPECTRAL INDEX AND COMPACTNESS FOR FRII SOURCES

Jenkins & McEllin (1977) showed that there is a correlation for FRII sources between luminosity and compactness, C, defined as

$$C = \frac{\text{Flux density in hot-spots of scale} < 15\ \text{kpc}}{\text{Total flux density} - \text{flux density of CC}} \quad \text{at 5 GHz.}$$

This was in the sense that C increased with luminosity, indicating that most of the emission of powerful sources comes from hot-spots, whereas less luminous sources have weak hot-spots. Fig. 8 shows a plot of α against C for all the FRII sources in the 178-MHz sample. The correlation between α and C for the identified sources is weaker than that between α and P_{1400}, so the spectral indices of FRII sources do not depend primarily on the fraction of flux density in hot-spots.

6 Discussion

We have investigated the relation between radio spectrum and radio luminosity for samples of extragalactic radio sources selected at 178 and 2700 MHz. High-resolution observations are available for all the objects studied and most have optical identifications. We can therefore exclude compact objects and subtract out the flux densities of any compact central components in the extended sources; we can also classify such objects by structural type. The completeness of the optical identifications means that high-power galaxies are not significantly discriminated against.

The correlation between spectral index and luminosity found by earlier workers is confirmed and is found to extend throughout the luminosity range, although it applies

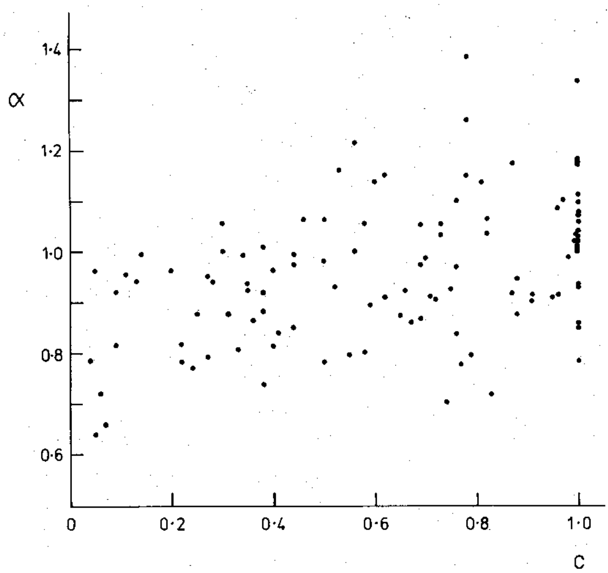

Figure 8. A plot of spectral index, α, against compactness, C, for all FRII sources in the 178-MHz sample. Central components have been subtracted.

principally to sources with hot-spots (FRII). As was pointed out by Bridle *et al.* (1972), this is not a selection effect caused by the spectral dependence of the radio K-correction which would favour the inclusion of flat-spectrum sources at high redshifts in a sample limited by flux density and lead to a correlation in the opposite sense to that observed. The correlation for FRII sources takes on added significance when we consider it in relation to two other observations. Firstly, where spectral index distributions within sources have been measured (e.g. Burch 1979b), the hot-spots are found to have spectra no steeper than the diffuse structure and often considerably flatter. Secondly, the hot-spots contribute a larger fraction of the total flux density in more luminous sources (Readhead & Longair 1975; Jenkins & McEllin 1977). From these two trends alone, one would expect more powerful sources to have flatter spectra than weaker sources. Thus, the observed correlation implies an even stronger relation between P and α for the hot-spots themselves.

We have also found relationships between the luminosity and the shape of the radio spectrum for FRII sources. Weak sources have spectra which steepen at low frequencies, possibly due to steep-spectrum components which are not visible on high-frequency maps. The spectra of the powerful sources show downward curvature at low frequencies; this is most marked for the most luminous sources. This effect has a natural explanation in that hot-spots are expected to be self-absorbed at $\nu < 100$ MHz; such regions are relatively more prominent in powerful sources in which the downward curvature of the total spectrum will therefore be greater. There is evidence for downward curvature in the spectra of some luminous FRII sources at high frequencies.

We may summarize the problems raised by this work as follows:

(1) The steep-spectrum components in weak sources (Section 4.2) should be observable by synthesis telescopes operating at low frequencies ($\nu < 200$ MHz).

(2) The range of frequencies available is insufficient to define high-frequency curvature in FRII sources with any precision.

(3) The P–α correlation needs to be investigated for types of source not well represented in our samples, for example the FRI and 'giant' ($D > 1$ Mpc) sources.

(4) The sources whose spectra are anomalously steep require further investigation to establish whether they form a distinct physical class.

(5) The scatter in the P–α relation for FRII sources appears to be smaller at low luminosities. This requires substantiation for a larger sample.

(6) The inferred correlation between P and α for hot-spots alone should be observable directly.

(7) To determine whether the above relations depend primarily on luminosity or on redshift requires a larger sample, selected to a much lower flux-density limit.

Acknowledgments

It is a pleasure to thank M. S. Longair, P. A. G. Scheuer, J. R. Shakeshaft and J. V. Wall for helpful discussions. We also thank the SRC for financial support.

References

Argue, A. N., Riley, J. M. & Pooley, G. G., 1978. *Observatory*, **98**, 132.
Artyukh, V. S., Vitkevich, V. V., Dagkesamanskii, R. D. & Kozhukhov, V. N., 1969. *Sov. Astr. A. J.*, **12**, 567.
Baars, J. W. M., Genzel, R., Pauliny-Toth, I. I. K. & Witzel, A., 1977. *Astr. Astrophys.*, **61**, 99.
Bennett, A. S., 1962. *Mem. R. astr. Soc.*, **68**, 163.
Bentley, M., Haves, P., Spencer, R. E. & Stannard, D., 1975. *Mon. Not. R. astr. Soc.*, **173**, 93P.
Bridle, A. H., 1967. *Observatory*, **87**, 60.
Bridle, A. H., Davis, M. M., Fomalont, E. B. & Lequeux, L., 1972. *Astr. J.*, **77**, 405.
Bridle, A. H. & Fomalont, E. B., 1978. *Astr. J.*, **83**, 704.
Bridle, A. H., Kesteven, M. J. L. & Guindon, B., 1972. *Astrophys. Lett.*, **11**, 27.
Bridle, A. H. & Purton, C. R., 1968. *Astr. J.*, **73**, 717.
Burch, S. F., 1977. *Mon. Not. R. astr. Soc.*, **181**, 599.
Burch, S. F., 1979a. *Mon. Not. R. astr. Soc.*, **186**, 293.
Burch, S. F., 1979b. *Mon. Not. R. astr. Soc.*, **186**, 519.
Burch, S. F., 1979c. *PhD Thesis*, University of Cambridge.
Caswell, J. L & Crowther, J. H., 1969. *Mon. Not. R. astr. Soc.*, **145**, 181.
De Young, D. S. & Hogg, D. E., 1973. *Astrophys. J. Lett.*, **180**, L61.
De Young, D. S., Hogg, D. E. & Wilkes, C. T., 1979. *Astrophys. J.*, **228**, 43.
Donaldson, W., Miley, G. K. & Palmer, H. P., 1971. *Mon. Not. R. astr. Soc.*, **152**, 145.
Fanaroff, B. L. & Riley, J. M., 1974. *Mon. Not. R. astr. Soc.*, **167**, 31P.
Genzel, R., Pauliny-Toth, I. I. K., Preuss, E. & Witzel, A., 1976. *Astr. J.*, **81**, 1084.
Ghigo, F. D., 1978. *Astr. J.*, **83**, 1363.
Heeschen, D. S., 1960. *Publs. astr. Soc. Pacif.*, **72**, 368.
Högbom, J. A. & Carlsson, I., 1974. *Astr. Astrophys.*, **34**, 341.
Jaffe, W. J. & Perola, G. C. 1974. *Astr. Astrophys.*, **31**, 223.
Jenkins, C. J. & McEllin, M., 1977. *Mon. Not. R. astr. Soc.*, **180**, 219.
Jenkins, C. J., Pooley, G. G. & Riley, J. M., 1977. *Mem. R. astr. Soc.*, **84**, 61.
Katgert, P., de Ruiter, H. R. & van der Laan, H., 1979. *Nature*, **280**, 20.
Kellermann, K. I. & Pauliny-Toth, I. I. K., 1973. *Astr. J.*, **78**, 828.
Kellermann, K. I., Pauliny-Toth, I. I. K. & Tyler, W. C., 1968. *Astr. J.*, **73**, 298.
Kellermann, K. I., Pauliny-Toth. I. I. K. & Williams, P. J. S., 1969. *Astrophys. J.*, **157**, 1.
Kristian, J., Sandage, A. & Katem, B., 1978. *Astrophys. J.*, **219**, 803.
Laing, R. A., Longair, M. S., Riley, J. M., Kibblewhite, E. J. & Gunn, J. E., 1978. *Mon. Not. R. astr. Soc.*, **183**, 547.
Macdonald, G. H., Kenderdine, S. & Neville, A. C., 1968. *Mon. Not. R. astr. Soc.*, **138**, 259.
Mackay, C. D., 1969. *Mon. Not. R. astr. Soc.*, **145**, 31.
Macleod, J. M. & Doherty, L. H., 1972. *Nature*, **238**, 88.
Meier, D. L., Ulrich, M-H., Fanti, R., Gioia, I. & Lari, C., 1979. *Astrophys. J.*, **229**, 25.
Menon, T. K., 1976. *Astrophys. J.*, **204**, 717.
Miley, G. K., 1971. *Mon. Not. R. astr. Soc.*, **152**, 477.
Northover, K. J. E., 1973. *Mon. Not. R. astr. Soc.*, **165**, 369.

Northover, K. J. E., 1976. *Mon. Not. R. astr. Soc.*, **177**, 307.
Pacholczyk, A. G., 1970. *Radio Astrophysics*, W. H. Freeman, San Francisco.
Pacholczyk, A. G., 1977. *Radio Galaxies*, Pergamon Press. Oxford.
Pauliny-Toth, I. I. K. & Kellermann, K. I., 1968. *Astr. J.*, **73**, 953.
Pauliny-Toth, I. I. K., Wade, C. M. & Heeschen, D. S., 1966. *Astrophys. J. Suppl. Ser.*, **13**, 65.
Pooley, G. G. & Henbest, S. N., 1974. *Mon. Not. R. astr. Soc.*, **169**, 477.
Readhead, A. C. S. & Longair, M. S., 1975. *Mon. Not. R. astr. Soc.*, **170**, 393.
Riley, J. M. & Branson, N. J. B. A., 1973. *Mon. Not. R. astr. Soc.*, **164**, 271.
Riley, J. M. & Pooley, G. G., 1976. *Mem. R. astr. Soc.*, **80**, 105.
Riley, J. M. & Pooley, G. G., 1978a. *Mon. Not. R. astr. Soc.*, **183**, 245.
Riley, J. M. & Pooley, G. G., 1978b. *Mon. Not. R. astr. Soc.*, **184**, 769.
Roger, R. S., Bridle, A. H. & Costain, C. H., 1973. *Astr. J.*, **78**, 1030.
Roger, R. S., Costain, C. H. & Lacey, J. D., 1969. *Astr. J.*, **74**, 36.
Schilizzi, R. T., 1976. *Astr. J.*, **81**, 946.
Scott, P. F. & Shakeshaft, J. R., 1971. *Mon. Not. R. astr. Soc.*, **155**, 19P.
Simon, A. J. B., 1978. *Mon. Not. R. astr. Soc.*, **184**, 537.
Smith, H. E., Junkkarinen, V., Spinrad, H., Grueff, G. & Vigotti, M., 1979. *Astrophys. J.*, **231**, 307.
Smith, H. E., Spinrad, H. & Smith, E. O., 1976. *Publs. astr. Soc. Pacif.*, **88**, 621.
Spinrad, H., 1978. *Astrophys. J. Lett.*, **220**, L35.
Spinrad, H., Westphal, J., Kristian, J. & Sandage, A., 1977. *Astrophys. J. Lett.*, **216**, L87.
Strom, R. G., Willis, A. G. & Wilson, A. S., 1978. *Astr. Astrophys.*, **68**, 367.
Stull, M. A., Price, K. M., D'Addario, L. R., Wernecke, S. J., Graff, W. & Grebenkemper, C. J., 1975. *Astr. J.*, **80**, 559.
Tabara, H. & Inoue, M., 1979. Preprint, Utsunomiya University, Japan.
Turland, B. D., 1975. *Mon. Not. R. astr. Soc.*, **170**, 281.
van Breugel, W. J. M., 1979. Preprint, Netherlands Foundation for Radio Astronomy.
van Breugel, W. J. M. & Miley, G. K., 1977. *Nature*, **265**, 315.
van der Laan, H. & Perola, G. C., 1969. *Astr. Astrophys.*, **3**, 468.
Véron, M. P., Véron, P. & Witzel, A., 1972. *Astr. Astrophys.*, **18**, 82.
Véron, M. P., Véron, P. & Witzel, A., 1974. *Astr. Astrophys. Suppl.*, **13**, 1.
Viner, M. R., 1975. *Astr. J.*, **80**, 83.
Viner, M. R. & Erickson, W. C., 1975. *Astr. J.*. **80**, 931.
Wills, B. J., 1973. *Astrophys. J.*, **180**, 335.

Appendix

Table A1. Morphological classification of low luminosity galaxies.

Source	Sample membership 178 MHz	2700 MHz	FR Class	Comments	References	α	$\log(P_{1400}/\mathrm{W\ Hz^{-1}\ sr^{-1}})$
3C 28	*		?		Riley & Pooley (1976)	1.239	26.59
3C 31	*	*	I	3C 31 Type	Burch (1977)	0.748^*	24.81
3C 35	*		?	Insufficient sensitivity	Mackay (1969)	0.893^*	25.68
3C 66B	*	*	I	3C 31 Type	Northover (1973)	0.810^*	25.27
3C 76.1	*	*		3C 31 Type	Macklin (in preparation)	0.645	25.14
3C 83.1B	*	*	I	Twin-tail	Riley & Pooley (1976)	0.692^*	25.10
0703+42		*	I	Twin-tail	Peacock (in preparation)	0.869^*	25.32
3C 264	*	*	I	3C 31 Type ?	Northover (1976)	0.908^*	25.03
3C 272.1	*	*	I	3C 31 Type	Jenkins <u>et al</u>. (1977)	0.634	23.42
3C 274	*	*	I	3C 31 Type	Turland (1975)	0.871	25.24
3C 288	*	*	?		Pooley & Henbest (1974)	0.983	27.04
3C 293	*	*	?	Double with extended structure	Argue, Riley & Pooley (1978)	0.710	25.62
3C 296	*	*	I	3C 31 Type	Birkinshaw, Laing & Peacock (in preparation)	0.632^*	25.01
3C 305	*	*	?	Double with extended structure	Pooley & Henbest (1974)	0.896	25.37

Table A1 – *continued*

Source	Sample membership 178 MHz	2700 MHz	FR Class	Comments	References	α	$\log(P_{1400}/\mathrm{W\,Hz^{-1}\,sr^{-1}})$
3C 310	*	*	?		van Breugel & Miley (1977)	1.300	26.02
3C 314.1	*		?	Two sources ?	Mackay (1969)	1.152	26.13
3C 315	*	*	?		Northover (1976)	0.945	26.33
3C 319	*	*	?		Jenkins, Pooley & Riley (1977)	1.031	26.68
1557+70		*	I	3C 31 Type	Peacock (in preparation)	0.912*	24.66
3C 338	*		?		Jaffe & Perola (1974)	1.682	25.14
3C 346	*	*	I	3C 31 Type	Pooley & Henbest (1974)	0.687	26.68
3C 386	*	*	?		Strom, Willis & Wilson (1978)	0.756	24.96
3C 433	*	*	?		Pooley & Henbest (1974)	0.907	26.76
3C 442A	*		?		Burch (1979c)	0.586*	25.02
3C 449	*	*	I	3C 31 Type	Birkinshaw, Laing & Peacock (in preparation)	0.672*	24.67
3C 465	*		I	Bent Double	Riley & Branson (1973)	0.928*	25.46

* in column 7 denotes that the flux densities may be in error because of resolution effects.

Notes to Table A1: Morphological Classification

3C 31 Type: An intense, collimated emitting region coincident with the galaxy, fading into diffuse outer structure.

Bent Double: Bright components on either side of the nucleus, with fainter regions further out.

Twin Tail: Two parallel streamers of emission stretching back from the galaxy, decreasing in brightness along their lengths.

Table A2. References for flux densities of central components.

Frequency/MHz	Reference
1400	Burch (1979a)
	Donaldson, Miley & Palmer (1971)
	Högbom & Carlsson (1974)
	Macdonald, Kenderdine & Neville (1968)
1666	Bentley et al. (1975)
2695	Birkinshaw, Laing & Peacock (in preparation)
	Bridle & Fomalont (1978)
	Burch (1977, 1979a)
	Laing (in preparation)
	Northover (1973, 1976)
4995	Jenkins, Pooley & Riley (1977) (and references therein)
8085	Bridle & Fomalont (1978)
	De Young & Hogg (1973)
	De Young, Hogg & Wilkes (1979)
	Ghigo (1978)
	Menon (1976)
	Schilizzi (1976)

Table A2 – *continued*

Frequency/MHz	Reference
10 700	Stull et al. (1975)
15 375	Burch (1977, 1979a)
	Laing (in preparation)
	Riley & Pooley (1978a,b)

14 900 and 10 700 MHz

The scales at these frequencies are based on the flux densities given by BGPW for Virgo A and Cyg A respectively at 14 900 and 10 700 MHz.

1400 MHz

The measurements by Bridle *et al.* (1972) were used whenever possible, supplemented by those of Pauliny-Toth *et al.* (1966), adjusted as described by KPW. Both sets of observations were made with linearly polarized feeds in P.A. 0°, and measured the Stokes parameter $I + Q$. We have converted to total intensity I using the polarization measurements listed by Tabara & Inoue (1979).

750 MHz

The observations by Pauliny-Toth *et al.* (1966) used linearly polarized feeds in P.A. 90°, measuring $I - Q$, but corrections for polarization have not been made because they are small (typically < 1 per cent) and very uncertain.

10, 22 and 26 MHz

At frequencies below 30 MHz, the fitted spectra given by BGPW for Cas A and Cyg A do not agree well with the absolute measurements. We have therefore based the calibration directly on the values of Bridle (1967), Roger, Costain & Lacy (1969) and Viner (1975), leaving the scales of RBC and Viner & Erickson (1975) unaltered. The scales at 22 and 26 MHz differ by 5 ± 2 per cent (Viner & Erickson 1975). This is insignificant compared with the errors in the individual flux densities. The spectral curvatures at low frequencies (Section 4.2) are too large to allow adjustment of these flux-density scales by extrapolation from higher frequencies.

38 and 178 MHz

The scales defined by KPW at 38 and 178 MHz are known to be non-linear in the sense that the flux densities of all sources apart from the very bright primary calibrators (Cas A, Cyg A and Tau A) are too low (e.g. Scott & Shakeshaft 1971). Various correction factors have been proposed; in particular, RBC obtained values of 1.18 ± 0.03 and 1.09 ± 0.03 at 38 and 178 MHz respectively by interpolation between 22.25 MHz and higher frequencies. As is shown in Section 4.2, the spectra of most sources are curved at low frequencies, so the most sensible way to determine such correction factors is to interpolate over as small a frequency range as possible, i.e. between 22 or 26 and 86 MHz for the 38-MHz scale. This procedure gives correction factors at 38 MHz of 1.12 ± 0.03 and 1.14 ± 0.03 respectively for those sources which have reliable flux-density measurements at all three frequencies. Similarly, a correction factor of 1.10 ± 0.03 at 178 MHz was derived by interpolation between 86 and 750 MHz. When the uncertainty of 3 per cent is considered in conjunction with the possible errors in the basic flux-density scales, the discrepancies between our values and those of RBC are not significant. For simplicity, we therefore adopted the scaling of RBC.

Comparison with other flux-density scales

It is of interest to compare our results with the flux-density scales of Véron, Véron & Witzel (1974), Wills (1973) and RBC. As is shown in Section 4.2, the spectra of most sources are curved at low frequencies, the amount and direction of curvature being correlated with luminosity. It is therefore unjustifiable to assume that the majority of sources have straight spectra as was done by Véron *et al.*

Our scaling factors agree within the errors with those of Wills (1973), once account is taken of the slightly different spectrum assumed for Cas A, except at 178 MHz. Here, the correction given by Wills is 1.225. We note, however, that those flux densities measured in the 4C pencil-beam survey (Caswell &

Crowther 1969) from which our 178-MHz flux densities have been taken whenever possible, the value becomes 1.13 ± 0.03 (3C 227, whose 178-MHz flux density is grossly discrepant, is excluded). This is in much better agreement with our value of 1.09.

The low-frequency scale adopted by RBC is identical to ours except at 86 MHz, where we have preferred to leave uncorrected the measurements of Artyukh *et al.* (1969). This is consistent with RBC's statement that their correction factor at 86 MHz is not significantly different from 1.

Table A3. Estimated redshifts and references to optical data.

Visual Magnitude V	Redshift z
19	0.30
19.5	0.36
20	0.44
20.5	0.54
21	0.66
21.5	0.80
22	0.98
22.5	1.20

Optical data are taken from Smith, Spinrad & Smith (1976) with additional redshifts from:

Kristian (private communication)

Smith *et al.* (1979)

Spinrad (1978)

Spinrad (private communication)

Spinrad *et al.* (1977)

and identifications from:

Jenkins, Pooley & Riley (1977)

Kristian, Sandage & Katem (1978)

Laing *et al.* (1978)

Longair, Riley & Gunn (in preparation)

Monthly Notices
of the
ROYAL
ASTRONOMICAL SOCIETY

VOL. 190, NO. 3, 1980

The relation between radio luminosity and spectrum for extended extragalactic radio sources

R. A. Laing and J. A. Peacock

Published for
the Royal Astronomical Society
by
Blackwell Scientific Publications Ltd
Osney Mead
Oxford
OX2 0EL

The microfiches are 105 × 148mm archivally permanent silver halide film produced to internationally accepted standards in the NMA 98-image format

Microfiches produced by Micromedia, Bicester, Oxon

We reproduce here the basic data for the 178 MHz sample used in this paper.

Table 1 gives total flux densities between 14900 MHz and 750 MHz scaled as described in section 3.1, together with their associated errors.

Columns	1 & 2	: Flux density and error at 14900 MHz
	3 & 4	- " - 10700
	5 & 6	- " - 5000
	7 & 8	- " - 2695
	9 & 10	- " - 1400
	11 & 12	- " - 750

Table 2 gives total flux densities between 178 MHz and 10 MHz, scaled as described in section 3.1, together with their associated errors.

Columns	1 & 2	: Flux density and error at 178 MHz
	3 & 4	- " - 86
	5 & 6	- " - 38
	7 & 8	- " - 26.3
	9 & 10	- " - 22.25
	11 & 12	- " - 10

Table 3 gives fitted spectral indices, with errors, and luminosities as used in section 5.

Columns	1 & 2	: Spectral index and error, evaluated using total flux densities
	3 & 4	P_{1400} and $\log_{10}(P_{1400})$, evaluated using total flux densities
	5 & 6	Spectral index and error, evaluated using CC-subtracted flux densities
	7 & 8	P_{1400} and $\log_{10}(P_{1400})$, evaluated using CC-subtracted flux densities

Table 1: High frequency flux densities.

		(1)	(2)	(3)	(4)	(5)	(6)	(7)	(8)	(9)	(10)	(11)	(12)
1	3C6.1	0.270	0.010	0.497	0.056	1.033	0.040	1.870	0.040	3.580	0.103	5.730	0.219
2	3C9	0.130	0.010	0.216	0.019	0.546	0.050	0.981	0.040	1.955	0.123	3.890	0.189
3	3C13	0.110	0.010	0.0	0.0	0.397	0.030	0.920	0.040	1.832	0.082	3.450	0.178
4	3C14	0.150	0.010	0.216	0.019	0.606	0.030	1.021	0.040	1.873	0.103	3.580	0.206
5	3C16	0.130	0.010	0.197	0.019	0.506	0.030	0.950	0.040	1.883	0.144	3.100	0.204
6	3C19	0.350	0.010	0.553	0.038	1.251	0.089	1.901	0.040	3.200	0.082	5.290	0.226
7	3C20	1.370	0.070	1.989	0.056	4.151	0.159	6.501	0.071	11.196	0.319	18.100	0.453
8	3C22	0.230	0.010	0.310	0.019	0.755	0.030	1.294	0.040	2.254	0.154	4.310	0.192
9	3C28	0.0	0.0	0.0	0.0	0.447	0.060	0.677	0.061	1.862	0.113	3.090	[illegible]
10	3C31	0.0	0.0	1.022	0.094	2.085	0.070	3.528	0.253	5.392	0.226	8.150	[illegible]
11	3C33	0.0	0.0	2.701	0.169	4.995	0.109	8.007	0.081	13.562	0.278	20.010	[illegible]
12	3C33.1	0.0	0.0	0.0	0.0	0.854	0.030	1.749	0.040	3.231	0.237	5.340	[illegible]
13	3C34	0.160	0.010	0.206	0.038	0.427	0.030	0.809	0.040	1.574	0.072	2.840	[illegible]
14	3C35	0.0	0.0	0.0	0.0	0.586	0.060	1.345	0.051	2.305	0.082	3.780	[illegible]
15	3C41	0.510	0.010	0.713	0.038	1.450	0.050	2.255	0.040	3.591	0.103	5.530	[illegible]
16	3C42	0.340	0.020	0.394	0.019	0.834	0.040	1.607	0.040	2.758	0.082	4.600	[illegible]
17	3C43	0.450	0.010	0.610	0.038	1.082	0.040	1.698	0.040	2.819	0.082	4.280	[illegible]
18	3C46	0.0	0.0	0.188	0.019	0.328	0.050	0.657	0.040	1.173	0.082	2.160	[illegible]
19	3C47	0.360	0.040	0.563	0.019	1.092	0.050	2.083	0.040	3.694	0.093	6.960	[illegible]
20	3C48	1.730	0.010	2.458	0.075	5.332	0.070	9.069	0.101	15.713	0.360	25.470	[illegible]
21	3C49	0.290	0.010	0.375	0.026	0.933	0.060	1.527	0.040	2.778	0.082	4.400	[illegible]
22	3C55	0.230	0.040	0.216	0.019	0.874	0.099	1.486	0.071	2.686	0.123	5.220	[illegible]
23	3C61.1	0.0	0.0	0.591	0.094	1.897	0.060	3.761	0.061	5.865	0.185	10.700	[illegible]
24	3C65	0.200	0.020	0.291	0.019	0.765	0.050	1.607	0.071	3.231	0.216	5.670	[illegible]
25	3C66B	0.0	0.0	0.0	0.0	2.820	0.129	5.227	0.121	9.364	0.412	12.300	[illegible]
26	3C67	0.300	0.010	0.413	0.028	0.904	0.050	1.698	0.040	3.046	0.237	4.710	[illegible]
27	3C68.1	0.230	0.010	0.328	0.019	0.824	0.030	1.395	0.040	2.490	0.165	4.350	[illegible]
28	3C68.2	0.0	0.0	0.033	0.014	0.179	0.030	0.415	0.040	1.050	0.072	2.450	[illegible]
29	3C76.1	0.0	0.0	0.619	0.075	1.301	0.040	1.961	0.040	2.974	0.072	4.430	[illegible]
30	3C79	0.320	0.030	0.563	0.019	1.301	0.040	2.477	0.040	4.466	0.412	8.850	[illegible]
31	3C83.1B	0.0	0.0	0.0	0.0	3.377	0.218	4.651	0.081	8.911	0.432	11.100	[illegible]
32	3C84	49.360	0.190	0.0	0.0	18.589	0.238	10.029	0.111	13.099	0.638	21.820	[illegible]
33	3C98	0.0	0.0	2.823	0.122	4.935	0.119	7.087	0.101	10.280	0.298	16.730	[illegible]
34	3C109	0.0	0.0	0.947	0.028	1.629	0.119	2.457	0.051	4.034	0.093	6.860	[illegible]
35	3C123	5.300	0.020	7.720	0.216	16.206	0.189	27.540	0.273	46.758	0.803	75.640	[illegible]
36	3C132	0.380	0.030	0.563	0.028	1.043	0.040	1.961	0.040	3.457	0.093	5.660	[illegible]
37	3C133	1.000	0.030	1.201	0.047	2.145	0.060	3.417	0.051	5.783	0.144	8.880	[illegible]
38	3C138	1.630	0.010	2.157	0.066	4.131	0.070	6.056	0.071	8.530	0.196	12.470	[illegible]
39	3C147	2.680	0.010	3.883	0.113	8.123	0.109	13.123	0.131	22.669	0.412	34.060	[illegible]
40	3C153	0.420	0.010	0.582	0.028	1.341	0.060	2.325	0.040	4.178	0.093	6.540	[illegible]
41	3C171	0.390	0.010	0.497	0.019	1.211	0.040	2.022	0.040	3.766	0.144	6.100	[illegible]
42	3C172	0.340	0.020	0.413	0.038	0.844	0.040	1.527	0.081	2.902	0.072	4.810	[illegible]
43	3C173.1	0.270	0.030	0.319	0.028	0.765	0.060	1.456	0.040	2.603	0.093	4.720	[illegible]
44	3C175	0.210	0.020	0.281	0.028	0.655	0.040	1.244	0.040	2.439	0.062	4.660	[illegible]
45	3C175.1	0.160	0.010	0.225	0.028	0.556	0.050	1.112	0.040	2.068	0.062	3.350	[illegible]
46	3C181	0.200	0.010	0.291	0.019	0.655	0.050	1.254	0.040	2.326	0.062	3.760	[illegible]
47	3C184	0.150	0.010	0.216	0.019	0.596	0.040	1.183	0.040	2.470	0.082	4.230	[illegible]
48	3C184.1	0.0	0.0	0.788	0.066	1.231	0.070	1.901	0.040	3.200	0.154	5.280	[illegible]
49	3C186	0.060	0.010	0.084	0.014	0.377	0.050	0.586	0.040	1.307	0.072	2.740	[illegible]
50	3C190	0.300	0.010	0.356	0.019	0.814	0.060	1.395	0.051	2.552	0.072	4.300	[illegible]
51	3C191	0.180	0.010	0.225	0.019	0.457	0.060	0.960	0.040	1.842	0.082	3.440	[illegible]
52	3C192	0.0	0.0	1.191	0.084	2.036	0.060	3.195	0.051	5.094	0.113	8.000	[illegible]
53	3C196	1.230	0.010	1.829	0.056	4.329	0.060	7.744	0.081	14.241	0.288	23.920	[illegible]
54	3C200	0.0	0.0	0.300	0.028	0.655	0.030	1.112	0.040	2.130	0.113	3.720	[illegible]
55	3C204	0.110	0.010	0.159	0.015	0.338	0.030	0.505	0.040	1.297	0.082	2.370	[illegible]
56	3C205	0.160	0.010	0.234	0.019	0.665	0.040	1.122	0.040	2.387	0.072	3.950	[illegible]
57	3C207	0.720	0.010	0.929	0.047	1.430	0.050	1.800	0.040	2.573	0.082	4.110	[illegible]
58	3C208	0.140	0.010	0.234	0.019	0.536	0.050	0.960	0.040	2.356	0.062	4.560	[illegible]

Table 1: High frequency flux densities.

		(1)	(2)	(3)	(4)	(5)	(6)	(7)	(8)	(9)	(10)	(11)	(12)
59	3C212	0.480	0.010	0.497	0.019	0.884	0.040	1.426	0.040	2.552	0.072	4.440	0.183
60	3C215	0.130	0.010	0.188	0.019	0.407	0.030	0.708	0.040	1.585	0.072	2.710	0.167
61	3C216	1.270	0.010	1.323	0.038	1.797	0.040	2.416	0.051	3.787	0.103	6.560	0.205
62	3C217	0.120	0.010	0.122	0.019	0.477	0.060	1.011	0.040	2.161	0.062	4.060	0.208
63	3C219	0.0	0.0	0.957	0.056	2.274	0.060	4.398	0.061	8.458	0.268	14.000	0.289
64	3C220.1	0.190	0.010	0.291	0.019	0.536	0.030	1.082	0.040	2.223	0.082	4.530	0.183
65	3C220.3	0.010	0.010	0.253	0.028	0.636	0.050	1.345	0.101	2.891	0.093	5.940	0.273
66	3C223	0.0	0.0	0.675	0.094	1.281	0.070	2.083	0.051	3.581	0.082	5.530	0.198
67	3C225B	0.310	0.020	0.431	0.019	0.824	0.070	1.516	0.202	3.396	0.309	5.200	0.500
68	3C226	0.140	0.010	0.197	0.019	0.636	0.050	1.183	0.040	2.387	0.062	4.610	0.176
69	3C228	0.360	0.020	0.553	0.028	1.132	0.050	2.002	0.040	3.602	0.082	5.710	0.183
70	3C231	1.730	0.030	2.204	0.056	3.912	0.079	5.651	0.101	8.170	0.175	10.710	0.278
71	3C234	0.500	0.040	0.760	0.028	1.529	0.050	1.952	0.051	5.546	0.123	9.910	0.234
72	3C239	0.080	0.010	0.122	0.019	0.328	0.030	0.657	0.040	1.461	0.072	2.960	0.188
73	3C241	0.070	0.010	0.113	0.028	0.338	0.050	0.738	0.040	1.688	0.082	3.100	0.165
74	3C244.1	0.320	0.030	0.478	0.019	1.112	0.040	1.971	0.040	3.941	0.093	6.840	0.199
75	3C245	0.850	0.010	0.965	0.038	1.380	0.040	2.113	0.040	3.283	0.082	5.060	0.178
76	3C247	0.250	0.010	0.375	0.028	0.943	0.060	1.648	0.040	2.953	0.123	4.780	0.194
77	3C249.1	0.310	0.020	0.375	0.019	0.775	0.030	1.415	0.040	2.315	0.082	3.690	0.175
78	3C250	0.090	0.010	0.094	0.014	0.288	0.030	0.495	0.040	1.276	0.113	2.630	0.185
79	3C252	0.130	0.030	0.113	0.015	0.318	0.030	0.586	0.040	1.214	0.082	2.670	0.166
80	3C254	0.200	0.010	0.300	0.019	0.784	0.050	1.456	0.040	1.252	0.134	5.430	0.184
81	3C263	0.230	0.020	0.535	0.019	1.033	0.040	1.749	0.040	3.108	0.113	5.130	0.207
82	3C263.1	0.0	0.0	0.339	0.019	0.375	0.030	1.607	0.051	3.046	0.072	5.700	0.195
83	3C264	0.0	0.0	1.013	0.028	1.986	0.070	3.266	0.051	5.917	0.298	9.620	0.257
84	3C265	0.210	0.030	0.281	0.019	0.526	0.030	1.405	0.040	2.840	0.082	5.290	0.192
85	3C266	0.120	0.010	0.113	0.019	0.318	0.040	0.586	0.040	1.482	0.082	2.750	0.167
86	3C267	0.230	0.030	0.319	0.019	0.586	0.070	1.304	0.040	2.161	0.072	4.160	0.181
87	3C268.1	0.940	0.070	1.276	0.038	2.602	0.060	4.044	0.081	6.761	0.134	10.020	0.260
88	3C268.3	0.330	0.010	0.478	0.038	1.082	0.040	2.002	0.040	3.622	0.154	5.670	0.195
89	3C268.4	0.180	0.010	0.244	0.019	0.596	0.030	1.072	0.040	2.068	0.093	3.620	0.174
90	3C270.1	0.440	0.010	0.450	0.019	0.864	0.040	1.506	0.040	2.727	0.072	5.040	0.191
91	3C272	0.160	0.020	0.169	0.015	0.357	0.030	0.708	0.040	1.760	0.144	2.500	0.184
92	3C272.1	1.300	0.050	0.820	0.056	2.840	0.079	3.953	0.061	6.472	0.237	8.850	0.229
93	3C274	28.400	0.420	35.550	0.976	71.556	0.993	119.571	1.213	220.206	9.261	337.000	17.000
94	3C274.1	0.0	0.0	0.394	0.038	0.755	0.030	1.456	0.040	2.778	0.082	5.120	0.182
95	3C275.1	0.520	0.010	0.722	0.056	0.904	0.060	1.577	0.040	2.953	0.072	5.040	0.186
96	3C277.2	0.180	0.030	0.206	0.019	0.576	0.030	0.920	0.040	1.852	0.062	3.040	0.188
97	3C277.3	0.520	0.030	0.638	0.028	1.231	0.040	1.951	0.040	2.933	0.082	4.280	0.182
98	3C280	0.520	0.020	0.722	0.028	1.519	0.060	2.861	0.051	5.124	0.113	8.150	0.213
99	3C280.1	0.110	0.010	0.131	0.015	0.357	0.030	0.627	0.040	1.451	0.072	2.590	0.186
100	3C284	0.0	0.0	0.263	0.019	0.685	0.060	1.082	0.040	1.852	0.072	3.140	0.165
101	3C285	0.0	0.0	0.450	0.038	0.755	0.050	1.244	0.040	2.037	0.062	3.140	0.172
102	3C286	3.460	0.030	4.390	0.122	7.478	0.089	10.373	0.111	14.632	0.309	19.230	0.340
103	3C287	1.420	0.030	1.726	0.047	3.237	0.060	4.651	0.061	6.803	0.144	9.570	0.251
104	3C288	0.240	0.010	0.347	0.019	0.983	0.060	1.779	0.040	3.406	0.093	6.140	0.189
105	3C289	0.180	0.010	0.244	0.019	0.596	0.030	1.183	0.040	2.346	0.072	4.090	0.181
106	3C293	0.740	0.020	0.078	0.028	1.857	0.040	2.922	0.051	4.558	0.113	7.200	0.220
107	3C294	0.060	0.010	0.087	0.014	0.278	0.040	0.546	0.040	1.358	0.072	2.440	0.370
108	3C295	1.600	0.020	2.589	0.075	6.484	0.079	11.960	0.121	22.823	0.401	36.930	0.615
109	3C296	0.0	0.0	1.022	0.103	1.698	0.050	2.730	0.051	4.229	0.185	5.450	0.203
110	3C299	0.260	0.010	0.366	0.019	0.894	0.050	1.607	0.040	3.056	0.103	4.970	0.290
111	3C300	0.310	0.020	0.478	0.028	1.092	0.040	1.941	0.040	3.602	0.082	6.420	0.209
112	3C303	0.610	0.010	0.610	0.028	0.933	0.060	1.567	0.040	2.665	0.072	4.060	0.181
113	3C303.1	0.100	0.010	0.188	0.019	0.457	0.050	0.617	0.040	1.893	0.113	2.920	0.176
114	3C305	0.310	0.010	0.441	0.038	0.914	0.040	1.658	0.040	3.025	0.093	2.020	0.190
115	3C305.1	0.100	0.030	0.215	0.019	0.457	0.030	0.778	0.040	1.729	0.113	2.510	0.174
116	3C309.1	1.500	0.040	2.420	0.084	3.734	0.069	5.358	0.071	8.201	0.185	15.490	0.273
117	3C310	0.0	0.0	0.338	0.028	1.271	0.070	3.215	0.051	7.892	0.278	15.910	0.358
118	3C314.1	0.0	0.0	0.131	0.028	0.328	0.030	0.708	0.040	1.616	0.113	2.950	0.180

Table 1: High frequency flux densities.

		(1)	(2)	(3)	(4)	(5)	(6)	(7)	(8)	(9)	(10)	(11)	(12)
119	3C315	0.0	0.0	0.694	0.047	1.261	0.040	2.386	0.040	4.116	0.103	6.950	0.236
120	3C318	0.230	0.010	0.319	0.019	0.745	0.030	1.345	0.040	2.562	0.072	4.440	0.183
121	3C319	0.220	0.030	0.281	0.019	0.645	0.030	1.264	0.040	2.500	0.062	4.550	0.183
122	3C321	0.390	0.020	0.525	0.028	1.211	0.040	2.052	0.040	3.571	0.082	6.240	0.198
123	3C322	0.100	0.020	0.278	0.015	0.457	0.030	3.859	0.040	1.976	0.134	3.460	0.182
124	3C324	0.140	0.010	0.225	0.019	0.605	0.030	1.274	0.040	2.439	0.062	4.720	0.176
125	3C325	0.250	0.020	0.394	0.019	0.824	0.040	1.860	0.040	3.776	0.123	6.190	0.194
126	3C330	0.630	0.040	0.957	0.028	2.334	0.079	3.801	0.051	6.925	0.165	10.890	0.342
127	3C334	0.310	0.020	0.310	0.019	0.556	0.030	1.335	0.040	2.151	0.134	3.490	0.183
128	3C336	0.210	0.010	0.356	0.019	0.685	0.060	1.405	0.040	2.737	0.072	4.360	0.197
129	3C337	0.320	0.030	0.460	0.019	0.904	0.030	1.567	0.101	2.943	0.072	5.240	0.226
130	3C338	0.150	0.020	0.169	0.019	0.487	0.030	1.354	0.040	2.653	0.093	9.190	0.236
131	3C340	0.240	0.020	0.272	0.019	0.685	0.030	1.555	0.040	2.490	0.062	3.690	0.176
132	3C341	0.200	0.030	0.234	0.019	0.566	0.040	2.092	0.040	2.151	0.093	7.540	0.183
133	3C343	0.350	0.020	0.557	0.028	0.480	0.040	2.709	0.051	5.320	0.144	7.940	0.243
134	3C343.1	0.350	0.010	0.460	0.019	1.192	0.040	2.255	0.051	4.826	0.103	8.000	0.236
135	3C345	8.540	0.050	0.0	0.0	5.610	0.079	6.076	0.071	6.791	0.165	7.930	0.190
136	3C346	0.750	0.010	0.816	0.028	1.519	0.099	2.256	0.051	3.807	0.144	5.720	0.179
137	3C349	0.460	0.060	0.544	0.019	3.132	0.040	2.901	0.040	3.375	0.082	4.960	0.183
138	3C351	0.420	0.020	0.553	0.028	0.202	0.050	2.052	0.040	3.622	0.103	5.160	0.170
139	3C352	0.150	0.020	0.216	0.019	0.467	0.030	0.960	0.040	1.965	0.072	3.460	0.171
140	3C356	0.0	0.0	0.122	0.014	0.377	0.040	0.657	0.040	1.410	0.113	2.840	0.171
141	3C368	0.0	0.0	0.070	0.019	0.209	0.030	0.435	0.040	1.111	0.103	2.500	0.272
142	3C380	3.040	0.020	0.0	0.0	7.447	0.089	9.089	0.121	14.602	0.298	23.180	0.409
143	3C381	0.530	0.040	0.741	0.028	2.281	0.050	2.025	0.040	3.879	0.185	5.720	0.299
144	3C382	0.0	0.0	1.425	0.038	2.204	0.070	3.328	0.051	5.834	0.463	9.290	0.270
145	3C386	0.0	0.0	1.398	0.075	3.562	0.079	3.368	0.081	7.162	0.257	10.990	[illegible]
146	3C388	0.580	0.030	0.891	0.047	1.758	0.040	3.144	0.051	5.742	0.237	9.750	[illegible]
147	3C390.3	0.0	0.0	2.401	0.094	4.449	0.079	6.632	0.071	11.257	0.576	17.590	[illegible]
148	3C401	0.430	0.010	0.528	0.038	1.360	0.050	2.790	0.101	4.877	0.144	8.180	0.613
149	3C427.1	0.270	0.020	0.394	0.028	0.953	0.060	1.911	0.040	3.931	0.082	7.230	0.232
150	3C432	0.080	0.010	0.131	0.015	3.308	0.050	0.758	0.040	1.502	0.113	2.900	0.167
151	3C433	1.220	0.040	1.717	0.047	0.724	0.070	6.551	0.071	11.782	0.278	20.840	0.433
152	3C436	0.260	0.030	0.441	0.019	0.983	0.030	1.840	0.040	2.396	0.093	5.740	0.187
153	3C437	0.300	0.020	0.394	0.019	0.273	0.060	1.527	0.040	2.758	0.072	5.050	0.182
154	3C438	0.390	0.010	0.500	0.019	0.579	0.060	3.255	0.051	6.894	0.144	13.700	0.370
155	3C441	0.270	0.020	0.403	0.028	0.914	0.030	1.527	0.040	2.521	0.082	4.240	0.101
156	3C442A	0.0	0.0	0.0	0.0	0.0	0.0	0.0	0.0	3.468	0.185	5.000	0.400
157	3C449	0.0	0.0	0.0	0.0	3.380	0.070	2.497	0.051	3.674	0.123	5.350	0.227
158	3C452	0.0	0.0	0.0	0.0	2.237	0.099	5.935	0.081	10.537	0.268	19.320	0.443
159	3C454	0.300	0.010	0.394	0.028	0.784	0.030	1.223	0.040	2.140	0.072	13.460	0.170
160	3C454.3	9.480	0.060	0.0	0.0	19.572	0.339	10.818	0.121	12.646	0.237	13.360	0.287
161	3C455	0.210	0.010	0.300	0.028	0.923	0.099	1.496	0.040	2.891	0.123	4.980	0.185
162	3C460	0.130	0.010	0.159	0.019	0.338	0.030	0.778	0.040	1.585	0.072	2.780	0.167
163	3C465	0.0	0.0	0.0	0.0	2.780	0.079	4.256	0.121	7.831	0.206	13.960	0.298
164	3C469.1	0.150	0.030	0.150	0.015	0.407	0.030	0.839	0.040	1.760	0.082	3.020	0.181
165	3C470	0.120	0.010	0.206	0.019	0.546	0.030	1.051	0.040	2.089	0.062	3.740	0.168

Table 2: Low frequency flux densities.

		(1)	(2)	(3)	(4)	(5)	(6)	(7)	(8)	(9)	(10)	(11)	(12)
1	3C6.1	18.857	1.886	30.500	2.300	0.0	0.0	0.0	0.0	71.300	14.999	0.0	0.0
2	3C9	19.402	0.970	35.700	1.600	75.520	7.552	99.000	18.000	97.750	16.667	204.000	42.000
3	3C13	13.080	0.654	20.600	1.900	67.260	13.452	46.000	7.000	0.0	0.0	0.0	0.0
4	3C14	11.336	1.134	24.400	2.700	42.480	8.496	69.000	7.000	0.0	0.0	0.0	0.0
5	3C15	12.208	0.610	21.200	1.100	36.580	7.316	99.000	9.000	74.750	11.667	0.0	0.0
6	3C19	13.189	1.319	21.700	5.500	41.300	12.390	44.000	6.000	72.450	8.333	0.0	0.0
7	3C20	46.761	2.358	74.000	3.800	132.160	39.660	152.000	13.000	154.100	16.667	246.000	72.000
8	3C22	13.189	0.659	25.300	1.600	47.200	14.160	76.000	9.000	62.100	5.000	168.000	30.000
9	3C28	17.767	1.777	42.100	2.700	89.680	8.968	115.000	9.000	167.900	25.000	0.0	0.0
10	3C31	18.312	0.916	34.000	1.600	63.720	6.372	65.000	7.000	86.250	25.000	144.000	48.000
11	3C33	59.296	2.965	107.000	3.000	161.660	8.083	222.000	26.000	270.250	46.667	588.000	120.000
12	3C33.1	14.170	1.417	28.700	3.000	48.380	9.676	0.0	0.0	0.0	0.0	0.0	0.0
13	3C34	22.971	1.297	28.900	2.300	74.340	7.434	86.000	13.000	69.000	14.999	240.000	72.000
14	3C35	11.445	1.144	24.100	1.600	64.900	6.490	47.000	6.000	62.100	16.667	186.000	36.000
15	3C41	11.554	1.155	19.600	1.200	43.660	8.732	0.0	0.0	72.450	18.333	0.0	0.0
16	3C42	13.080	0.654	21.200	1.200	41.300	8.260	41.000	6.000	0.0	0.0	0.0	0.0
17	3C43	12.644	1.264	20.500	4.400	46.020	9.204	46.000	6.000	69.000	8.333	0.0	0.0
18	3C46	11.118	0.556	22.600	1.200	38.940	7.788	58.000	6.000	74.750	14.999	0.0	0.0
19	3C47	28.776	2.878	62.100	6.800	147.500	14.750	190.000	13.000	254.150	18.333	312.000	72.000
20	3C48	59.950	2.998	80.400	2.300	71.980	7.198	37.000	6.000	55.200	6.667	0.0	0.0
21	3C49	11.227	0.561	15.200	1.100	0.0	0.0	0.0	0.0	0.0	0.0	0.0	0.0
22	3C55	34.743	2.474	43.500	1.600	89.680	8.968	88.000	7.000	0.0	0.0	180.000	72.000
23	3C61.1	34.008	3.401	63.000	15.000	102.660	10.266	0.0	0.0	125.350	50.000	0.0	0.0
24	3C65	0.0	0.0	0.0	0.0	0.0	0.0	0.0	0.0	0.0	0.0	0.0	0.0
25	3C66B	38.913	1.946	0.0	0.0	147.500	7.375	0.0	0.0	345.000	44.999	672.000	120.000
26	3C67	10.900	0.545	24.900	1.100	0.0	0.0	0.0	0.0	0.0	0.0	0.0	0.0
27	3C68.1	13.952	1.395	39.900	1.600	55.460	5.546	88.000	6.000	79.350	10.000	156.000	30.000
28	3C68.2	14.170	1.417	32.500	2.200	74.340	7.434	92.000	9.000	0.0	0.0	222.000	60.000
29	3C76.1	13.298	0.665	20.600	2.200	29.500	8.850	41.000	7.000	0.0	0.0	0.0	0.0
30	3C79	33.245	1.662	58.600	1.200	88.500	8.850	154.000	9.000	119.600	14.999	252.000	66.000
31	3C83.1B	0.0	0.0	0.0	0.0	0.0	0.0	0.0	0.0	0.0	0.0	0.0	0.0
32	3C84	68.234	3.412	147.000	6.600	424.800	21.240	751.000	48.000	819.950	88.334	1704.000	384.000
33	3C98	51.443	2.572	94.300	2.200	173.460	8.673	215.000	18.000	311.650	43.333	252.000	66.000
34	3C109	23.544	1.177	44.000	2.200	69.620	6.962	117.000	9.000	129.950	35.000	210.000	54.000
35	3C123	206.010	10.301	391.000	9.000	680.860	34.043	828.000	39.000	911.949	63.333	960.000	192.000
36	3C132	14.933	0.747	34.100	1.100	51.920	5.192	63.000	8.000	56.350	13.333	0.0	0.0
37	3C133	24.307	1.215	35.800	4.200	68.440	6.844	97.000	21.000	80.550	18.333	120.000	36.000
38	3C136	24.198	1.210	34.800	3.000	15.340	5.369	0.0	0.0	0.0	0.0	0.0	0.0
39	3C147	45.945	2.297	60.000	3.000	21.240	6.372	39.000	7.000	0.0	0.0	0.0	0.0
40	3C153	16.677	0.834	26.200	1.100	47.200	4.720	42.000	8.000	302.450	66.667	0.0	0.0
41	3C171	21.255	1.063	34.800	1.900	57.820	5.782	97.000	10.000	83.950	10.000	0.0	0.0
42	3C172	16.459	1.645	22.800	1.100	48.380	4.838	71.000	6.000	69.000	6.667	156.000	48.000
43	3C173.1	16.786	0.830	37.300	1.100	56.640	5.664	0.0	0.0	0.0	0.0	0.0	0.0
44	3C175	19.184	0.959	30.700	3.400	95.580	9.558	132.000	10.000	129.950	14.999	210.000	78.000
45	3C175.1	22.426	0.621	20.200	1.600	22.420	6.726	0.0	0.0	0.0	0.0	0.0	0.0
46	3C181	15.805	0.790	24.200	2.200	37.760	7.552	57.000	8.000	0.0	0.0	0.0	0.0
47	3C184	14.388	0.719	23.800	2.700	35.400	7.080	0.0	0.0	0.0	0.0	0.0	0.0
48	3C184.1	16.170	1.417	33.000	1.700	43.660	4.366	0.0	0.0	59.800	6.667	0.0	0.0
49	3C186	15.369	0.768	33.200	2.700	57.820	5.782	54.000	7.000	54.050	5.000	0.0	0.0
50	3C190	16.350	0.818	26.800	2.700	40.120	8.024	64.000	8.000	71.300	11.667	192.000	42.000
51	3C191	14.170	0.709	34.300	1.600	56.640	5.664	46.000	8.000	96.600	11.667	276.000	66.000
52	3C192	22.890	3.289	47.500	5.000	93.220	9.322	136.000	9.000	131.100	11.667	186.000	48.000
53	3C196	74.338	3.217	123.000	6.000	195.880	9.794	218.000	14.000	278.300	28.334	408.000	84.000
54	3C200	15.260	0.526	25.200	2.200	48.380	4.838	68.000	6.000	0.0	0.0	168.000	42.000
55	3C204	11.445	0.572	29.600	1.100	53.100	5.310	0.0	0.0	0.0	0.0	0.0	0.0
56	3C205	13.734	1.373	39.200	4.400	54.280	5.428	60.000	10.000	0.0	0.0	162.000	36.000
57	3C207	14.824	0.741	34.800	1.700	43.660	8.732	61.000	7.000	0.0	0.0	0.0	0.0
58	3C208	20.165	1.008	41.500	2.400	68.440	6.844	63.000	10.000	67.850	21.667	0.0	0.0

Table 2: Low frequency flux densities.

		(1)	(2)	(3)	(4)	(5)	(6)	(7)	(8)	(9)	(10)	(11)	(12)
59	3C212	16.459	0.823	29.800	3.100	25.960	7.788	51.000	7.000	29.900	11.667	0.0	0.0
60	3C215	12.426	0.621	30.700	3.000	42.480	8.496	66.000	8.000	0.0	0.0	168.000	48.000
61	3C216	22.018	[illegible]	52.600	4.500	60.180	6.018	88.000	7.000	118.450	35.000	0.0	0.0
62	3C217	[illegible]	[illegible]	24.400	1.300	46.020	4.602	43.000	6.000	0.0	0.0	0.0	0.0
63	3C219	[illegible]	[illegible]	81.100	3.900	139.240	6.962	212.000	11.000	202.400	36.667	396.000	90.000
64	3C220.1	[illegible]	[illegible]	59.800	5.000	54.280	5.428	0.0	0.0	0.0	0.0	0.0	0.0
65	3C220.3	[illegible]	[illegible]	51.600	9.900	49.560	4.956	0.0	0.0	0.0	0.0	0.0	0.0
66	3C225B	[illegible]	[illegible]	27.600	1.100	51.920	5.192	82.000	7.000	0.0	0.0	0.0	0.0
67	3C226	0.0	0.0	0.0	0.0	0.0	0.0	0.0	0.0	0.0	0.0	0.0	0.0
68	3C228	[illegible]	[illegible]	35.500	1.100	56.640	5.664	97.000	9.000	0.0	0.0	0.0	0.0
69	[illegible]	[illegible]	[illegible]	33.800	1.300	53.100	5.310	68.000	8.000	105.800	10.000	198.000	42.000
70	[illegible]	[illegible]	[illegible]	27.800	3.800	27.140	5.428	0.0	0.0	39.100	6.667	0.0	0.0
71	[illegible]	[illegible]	[illegible]	67.700	3.400	134.520	13.452	177.000	12.000	224.250	51.667	408.000	96.000
72	[illegible]	[illegible]	[illegible]	25.800	1.600	59.000	5.900	78.000	8.000	81.650	10.000	0.0	0.0
73	[illegible]	[illegible]	[illegible]	19.800	1.100	0.0	0.0	0.0	0.0	0.0	0.0	0.0	0.0
74	[illegible]	[illegible]	[illegible]	39.400	4.600	80.140	8.614	99.000	10.000	0.0	0.0	216.000	42.000
75	[illegible]	[illegible]	[illegible]	27.400	1.100	47.200	4.720	73.000	8.000	64.400	11.667	170.400	33.600
76	[illegible]	[illegible]	[illegible]	15.700	2.200	25.960	5.192	29.000	7.000	48.300	6.667	110.400	34.800
77	[illegible]	[illegible]	[illegible]	27.600	1.300	46.020	9.204	0.0	0.0	0.0	0.0	0.0	0.0
78	[illegible]	[illegible]	[illegible]	35.200	4.100	56.640	5.664	105.000	8.000	108.100	28.334	360.000	84.000
79	[illegible]	[illegible]	[illegible]	31.400	1.900	79.060	7.906	96.000	8.000	0.0	0.0	144.000	48.000
80	[illegible]	[illegible]	[illegible]	53.900	2.700	71.980	7.198	95.000	8.000	156.400	43.333	192.000	36.000
81	[illegible]	[illegible]	[illegible]	34.400	1.100	54.280	5.428	0.0	0.0	0.0	0.0	0.0	0.0
82	[illegible]	[illegible]	[illegible]	33.300	2.300	53.100	5.310	0.0	0.0	0.0	0.0	0.0	0.0
83	[illegible]	[illegible]	[illegible]	61.000	4.200	113.280	11.328	141.000	10.000	293.250	33.334	756.000	150.000
84	[illegible]	[illegible]	[illegible]	42.100	1.900	90.860	9.086	129.000	7.000	127.650	21.667	0.0	0.0
85	[illegible]	[illegible]	[illegible]	22.800	1.100	33.040	6.608	33.000	8.000	0.0	0.0	0.0	0.0
86	[illegible]	[illegible]	[illegible]	27.500	1.100	48.380	9.676	69.000	7.000	0.0	0.0	0.0	0.0
87	[illegible]	[illegible]	[illegible]	43.000	2.300	60.180	6.018	0.0	0.0	0.0	0.0	222.000	60.000
88	[illegible]	[illegible]	[illegible]	21.900	2.200	0.0	0.0	0.0	0.0	0.0	0.0	0.0	0.0
89	[illegible]	[illegible]	[illegible]	22.400	2.700	36.580	7.316	34.000	8.000	0.0	0.0	0.0	0.0
90	[illegible]	[illegible]	[illegible]	30.800	2.700	33.040	6.608	60.000	8.000	60.950	10.000	0.0	0.0
91	[illegible]	[illegible]	[illegible]	19.500	1.100	18.880	6.608	35.000	6.000	34.500	5.000	0.0	0.0
92	[illegible]	[illegible]	[illegible]	0.0	0.0	54.280	10.856	0.0	0.0	0.0	0.0	0.0	0.0
93	3C274	[illegible]	[illegible]	0.0	0.0	4212.598	210.630	4341.000	232.000	5611.996	499.999	9959.996	2400.000
94	3C274.1	[illegible]	[illegible]	39.000	2.200	68.440	6.844	113.000	24.000	0.0	0.0	0.0	0.0
95	3C275	[illegible]	[illegible]	36.400	1.100	47.200	9.440	0.0	0.0	46.000	8.333	0.0	0.0
96	3C275.1	[illegible]	[illegible]	25.200	2.200	56.640	11.328	62.000	8.000	0.0	0.0	0.0	0.0
97	3C277.3	[illegible]	[illegible]	27.000	2.700	38.940	7.788	40.000	6.000	0.0	0.0	0.0	0.0
98	3C280	[illegible]	[illegible]	45.000	3.400	73.160	7.316	94.000	10.000	149.500	21.667	192.000	36.000
99	3C280.1	[illegible]	[illegible]	26.700	1.900	31.860	6.372	41.000	6.000	0.0	0.0	0.0	0.0
100	3C284	[illegible]	[illegible]	29.000	4.100	54.280	5.428	81.000	6.000	87.400	8.333	126.000	30.000
101	3C285	[illegible]	[illegible]	23.400	1.900	42.480	4.248	0.0	0.0	51.750	8.333	0.0	0.0
102	3C286	[illegible]	[illegible]	32.900	1.900	37.760	7.552	34.000	8.000	59.800	13.333	85.200	25.200
103	3C287	[illegible]	[illegible]	19.400	2.200	30.680	6.136	0.0	0.0	0.0	0.0	0.0	0.0
104	3C288	[illegible]	[illegible]	18.600	1.600	55.460	5.546	97.000	6.000	74.750	11.667	159.600	50.400
105	3C289	[illegible]	[illegible]	21.100	2.200	34.220	5.422	33.000	8.000	0.0	0.0	0.0	0.0
106	3C293	[illegible]	[illegible]	27.400	1.900	49.560	4.956	44.000	6.000	65.550	11.667	170.400	34.800
107	3C294	[illegible]	[illegible]	27.900	1.600	74.340	7.434	69.000	7.000	0.0	0.0	0.0	0.0
108	3C295	[illegible]	[illegible]	133.000	3.000	110.920	5.546	72.000	10.000	66.700	25.000	0.0	0.0
109	3C296	[illegible]	[illegible]	29.100	2.200	30.680	9.204	0.0	0.0	0.0	0.0	0.0	0.0
110	3C299	[illegible]	[illegible]	20.500	1.100	34.220	6.844	0.0	0.0	0.0	0.0	0.0	0.0
111	3C300	[illegible]	[illegible]	37.100	5.300	79.060	7.906	96.000	8.000	121.900	18.333	288.000	80.000
112	3C303	[illegible]	[illegible]	33.000	2.200	43.660	4.366	50.000	10.000	0.0	0.0	0.0	0.0
113	3C303.1	[illegible]	[illegible]	15.800	2.700	15.340	5.369	0.0	0.0	0.0	0.0	0.0	0.0
114	3C305	[illegible]	[illegible]	37.400	1.900	57.820	5.782	0.0	0.0	0.0	0.0	0.0	0.0
115	3C305.1	[illegible]	[illegible]	14.000	1.700	15.340	5.369	0.0	0.0	0.0	0.0	0.0	0.0
116	3C309.1	[illegible]	[illegible]	52.500	3.300	43.660	4.366	0.0	0.0	50.600	6.667	0.0	0.0
117	3C310	[illegible]	0.052	129.000	4.000	257.240	12.862	382.000	31.000	385.250	33.334	600.000	168.000
118	3C314.1	[illegible]	0.578	25.600	2.800	50.740	5.074	0.0	0.0	96.600	8.333	0.0	0.0

Table 2: Low frequency flux densities.

		(1)	(2)	(3)	(4)	(5)	(6)	(7)	(8)	(9)	(10)	(11)	(12)
119	3C315	20.601	2.060	48.800	1.900	86.140	8.614	133.000	9.000	0.0	0.0	198.000	66.000
120	3C318	13.407	0.670	23.500	1.100	25.950	7.788	131.000	7.000	37.950	3.334	0.0	0.0
121	3C319	16.677	0.834	30.800	1.000	55.460	5.546	91.000	9.000	80.500	8.333	150.000	76.000
122	3C321	14.715	1.472	33.900	3.200	58.440	6.844	107.000	8.000	110.400	13.333	204.000	54.000
123	3C322	11.009	0.550	25.400	2.000	34.220	5.422	0.0	0.0	0.0	0.0	132.000	24.000
124	3C324	17.222	0.861	55.800	1.500	57.820	5.782	63.000	7.000	0.0	0.0	0.0	0.0
125	3C325	17.004	0.850	33.100	1.700	42.480	4.248	0.0	0.0	0.0	0.0	0.0	0.0
126	3C330	30.302	1.515	50.800	3.300	95.580	9.358	0.0	0.0	90.850	8.333	110.400	60.000
127	3C334	11.881	0.594	29.300	1.900	43.780	4.378	82.000	6.000	86.250	8.333	0.0	0.0
128	3C336	12.535	1.253	30.000	1.800	47.200	6.720	64.000	7.000	82.800	6.667	192.000	60.000
129	3C337	12.862	0.643	30.200	1.100	33.040	6.608	82.000	12.000	85.100	36.667	192.000	60.000
130	3C338	51.121	2.556	106.000	3.000	259.600	12.980	314.000	14.000	334.650	21.667	408.000	78.000
131	3C340	11.009	0.550	20.700	2.200	42.480	8.496	41.000	6.000	0.0	0.0	0.0	0.0
132	3C341	11.772	1.177	15.400	1.000	42.480	8.496	65.000	6.000	0.0	0.0	0.0	0.0
133	3C343	13.516	0.676	15.700	1.600	0.0	0.0	0.0	0.0	0.0	0.0	0.0	0.0
134	3C343.1	12.535	0.627	25.400	1.900	29.440	3.504	0.0	0.0	0.0	0.0	0.0	0.0
135	3C345	11.772	0.589	25.400	1.300	28.320	5.664	34.000	6.000	0.0	0.0	0.0	0.0
136	3C346	11.881	0.594	35.100	1.000	41.300	5.260	0.0	0.0	0.0	0.0	0.0	0.0
137	3C349	14.497	0.725	25.500	1.700	59.000	5.900	0.0	0.0	0.0	0.0	0.0	0.0
138	3C351	14.933	0.747	35.100	1.000	47.200	4.720	0.0	0.0	49.450	5.000	0.0	0.0
139	3C352	12.317	0.616	25.300	2.700	45.560	9.912	70.000	25.000	49.450	6.667	0.0	0.0
140	3C356	12.317	0.616	23.300	1.600	55.640	5.664	69.000	10.000	49.450	13.333	110.400	30.000
141	3C368	15.042	0.752	29.200	1.500	63.720	10.116	95.000	10.000	129.950	18.333	0.0	0.0
142	3C380	64.746	3.237	121.000	1.900	248.980	12.449	271.000	23.000	343.850	21.667	168.000	30.000
143	3C381	18.094	0.905	37.000	2.030	41.300	4.130	80.000	13.000	0.0	0.0	0.0	0.0
144	3C382	21.691	1.085	47.000	2.700	108.560	5.712	108.000	11.000	134.550	14.999	0.0	0.0
145	3C386	26.051	1.303	30.500	1.900	84.960	7.486	91.000	13.000	109.250	46.667	0.0	0.0
146	3C388	26.814	1.341	22.500	1.900	75.700	7.670	111.000	19.000	92.000	10.000	175.200	85.200
147	3C390.3	51.775	2.589	92.500	2.200	141.600	42.480	0.0	0.0	277.150	46.667	0.0	0.0
148	3C401	22.781	1.139	40.600	4.400	0.0	0.0	0.0	0.0	55.200	13.333	0.0	0.0
149	3C427.1	28.994	1.450	58.900	4.300	109.740	32.922	0.0	0.0	166.750	16.667	0.0	0.0
150	3C432	11.990	1.199	21.100	4.200	55.460	11.092	42.000	7.000	65.550	8.333	0.0	0.0
151	3C433	61.258	3.063	110.000	1.900	220.660	65.998	267.000	16.000	190.900	16.667	0.0	0.0
152	3C436	19.402	0.970	61.300	4.000	102.560	30.798	113.000	10.000	108.100	11.667	0.0	0.0
153	3C437	15.914	0.796	45.200	2.200	50.740	10.148	46.000	8.000	0.0	0.0	0.0	0.0
154	3C438	48.723	2.436	26.700	1.000	162.840	48.852	228.000	12.000	233.450	20.000	144.000	36.000
155	3C441	13.734	1.373	27.700	1.500	48.380	9.676	58.000	7.000	54.050	5.000	0.0	0.0
156	3C442A	0.0	0.0	0.0	0.0	0.0	0.0	0.0	0.0	0.0	0.0	0.0	0.0
157	3C449	12.535	0.627	29.900	3.100	0.0	0.0	0.0	0.0	0.0	0.0	0.0	0.0
158	3C452	59.296	2.965	114.000	3.000	236.000	70.800	288.000	18.000	331.200	21.667	396.000	108.000
159	3C454	12.644	0.632	0.0	0.0	31.860	9.558	0.0	0.0	0.0	0.0	0.0	0.0
160	3C454.3	14.170	0.709	36.600	5.000	31.860	6.372	0.0	0.0	0.0	0.0	0.0	0.0
161	3C455	13.952	0.698	20.900	3.900	48.380	4.838	0.0	0.0	0.0	0.0	0.0	0.0
162	3C460	11.227	2.245	0.0	0.0	0.0	0.0	0.0	0.0	0.0	0.0	0.0	0.0
163	3C465	41.202	2.060	91.500	2.200	147.500	29.500	194.000	23.000	233.450	53.334	480.000	84.000
164	3C469.1	13.516	1.352	32.300	1.100	0.0	0.0	0.0	0.0	0.0	0.0	0.0	0.0
165	3C470	11.009	0.550	14.700	1.100	0.0	0.0	0.0	0.0	57.500	5.000	0.0	0.0

Table 3: Spectral indices and luminosities.

		(1)	(2)	(3)	(4)	(5)	(6)	(7)	(8)
1	3C6.1	0.91	0.04	.207E+29	28.316	0.91	0.04	.207E+29	28.316
2	3C9	1.06	0.02	.146E+30	29.165	1.06	0.02	.146E+30	29.165
3	3C13	1.10	0.06	.640E+28	27.806	1.10	0.06	.640E+28	27.806
4	3C14	0.93	0.03	.227E+28	27.356	0.93	0.03	.227E+28	27.356
5	3C16	0.96	0.03	.613E+28	27.787	0.96	0.03	.613E+28	27.787
6	3C19	0.79	0.02	.453E+28	27.656	0.79	0.02	.453E+28	27.656
7	3C20	0.79	0.02	.767E+28	27.885	0.79	0.02	.767E+28	27.885
8	3C22	0.92	0.02	.717E+28	27.855	0.92	0.02	.717E+28	27.855
9	3C28	1.24	0.10	.384E+27	26.585	1.24	0.10	.384E+27	26.585
10	3C31	0.72	0.02	.655E+25	24.817	0.75	0.02	.638E+25	24.805
11	3C33	0.74	0.03	.216E+27	26.334	0.74	0.03	.216E+27	26.334
12	3C33.1	0.99	0.08	.542E+27	26.734	0.99	0.08	.542E+27	26.734
13	3C34	1.01	0.01	.525E+28	27.720	1.01	0.01	.525E+28	27.720
14	3C35	0.89	0.10	.473E+26	25.675	0.89	0.10	.473E+26	25.675
15	3C41	0.71	0.0	.103E+29	28.012	0.71	0.0	.103E+29	28.012
16	3C42	0.87	0.05	.256E+28	27.408	0.87	0.05	.256E+28	27.408
17	3C43	0.74	0.02	.610E+29	28.785	0.74	0.02	.610E+29	28.785
18	3C46	0.95	0.03	.141E+28	27.149	0.95	0.03	.141E+28	27.149
19	3C47	0.95	0.03	.415E+28	27.618	0.98	0.03	.412E+28	27.615
20	3C48	0.83	0.01	.121E+29	28.083	0.83	0.01	.121E+29	28.083
21	3C49	0.84	0.03	.850E+28	27.930	0.84	0.03	.850E+28	27.930
22	3C55	0.97	0.03	.330E+28	27.518	0.97	0.03	.330E+28	27.518
23	3C61.1	0.87	0.08	.997E+27	26.999	0.87	0.08	.997E+27	26.999
24	3C65	1.03	0.04	.0	0.0	1.03	0.04	.0	0.0
25	3C66B	0.78	0.09	.190E+26	25.278	0.81	0.09	.184E+26	25.265
26	3C67	0.84	0.05	.161E+28	27.207	0.84	0.05	.161E+28	27.207
27	3C68.1	0.88	0.01	.391E+29	28.592	0.88	0.01	.391E+29	28.592
28	3C68.2	1.38	0.01	.0	0.0	1.38	0.01	.0	0.0
29	3C76.1	0.64	0.01	.137E+26	25.138	0.64	0.01	.137E+26	25.138
30	3C79	1.01	0.02	.161E+28	27.206	1.01	0.02	.161E+28	27.206
31	3C83.1B	0.69	0.07	.127E+26	25.105	0.69	0.07	.127E+26	25.104
32	3C84	0.03	0.38	.167E+26	25.223	0.03	0.38	.167E+26	25.223
33	3C98	0.64	0.03	.423E+26	25.626	0.64	0.03	.423E+26	25.626
34	3C109	0.79	0.03	.204E+28	27.309	0.89	0.02	.197E+28	27.295
35	3C123	0.81	0.02	.114E+29	28.055	0.81	0.02	.114E+29	28.055
36	3C132	0.88	0.04	.816E+27	26.912	0.88	0.04	.816E+27	26.912
37	3C133	0.76	0.02	.169E+29	28.229	0.80	0.01	.167E+29	28.223
38	3C138	0.58	0.02	.317E+29	28.501	0.58	0.02	.317E+29	28.501
39	3C147	0.77	0.02	.424E+29	28.628	0.77	0.02	.424E+29	28.628
40	3C153	0.84	0.03	.172E+28	27.235	0.84	0.03	.172E+28	27.235
41	3C171	0.86	0.02	.112E+28	27.050	0.86	0.02	.112E+28	27.050
42	3C172	0.92	0.04	.927E+28	27.967	0.92	0.04	.927E+28	27.967
43	3C173.1	0.93	0.02	.123E+28	27.091	0.93	0.02	.123E+28	27.091
44	3C175	1.03	0.0	.121E+29	28.083	1.06	0.0	.121E+29	28.083
45	3C175.1	0.92	0.06	.0	0.0	0.92	0.06	.0	0.0
46	3C181	0.91	0.05	.504E+29	28.703	0.91	0.05	.504E+29	28.703
47	3C184	1.03	0.05	.402E+29	28.605	1.03	0.05	.402E+29	28.605
48	3C184.1	0.78	0.02	.211E+27	26.324	0.78	0.02	.211E+27	26.324
49	3C186	1.13	0.08	.164E+29	28.215	1.13	0.08	.164E+29	28.215
50	3C190	0.88	0.02	.354E+29	28.548	0.88	0.02	.354E+29	28.548
51	3C191	1.02	0.03	.119E+30	29.075	1.02	0.03	.119E+30	29.075
52	3C192	0.72	0.0	.821E+26	25.915	0.72	0.0	.821E+26	25.915
53	3C196	0.90	0.02	.903E+29	28.956	0.90	0.02	.903E+29	28.956
54	3C200	0.92	0.02	.283E+28	27.451	1.00	0.01	.276E+28	27.441
55	3C204	1.08	0.10	.178E+29	28.250	1.15	0.09	.184E+29	28.265
56	3C205	0.98	0.07	.744E+29	28.871	0.99	0.06	.741E+29	28.870
57	3C207	0.55	0.07	.737E+28	27.867	0.79	0.03	.667E+28	27.824
58	3C208	1.19	0.07	.347E+29	28.541	1.26	0.07	.344E+29	28.537

Table 3: Spectral indices and luminosities.

		(1)	(2)	(3)	(4)	(5)	(6)	(7)	(8)
59	3C212	0.86	0.02	.251E+29	28.399	1.03	0.01	.255E+29	28.407
60	3C215	1.04	0.06	.170E+28	27.230	1.06	0.06	.168E+28	27.227
61	3C216	0.67	0.07	.110E+29	28.041	0.67	0.07	.110E+29	28.041
62	3C217	1.11	0.04	.214E+29	28.331	1.11	0.04	.214E+29	28.331
63	3C219	0.94	0.04	.130E+28	27.113	0.96	0.04	.129E+28	27.110
64	3C220.1	1.12	0.01	.474E+28	27.676	1.15	0.01	.474E+28	27.676
65	3C220.3	1.17	0.01	.0	0.0	1.17	0.01	.0	0.0
66	3C223	0.78	0.03	.320E+27	26.506	0.79	0.02	.319E+27	26.503
67	3C225B	1.00	0.07	.688E+28	27.838	1.00	0.07	.688E+28	27.838
68	3C226	1.06	0.01	.228E+29	28.358	1.06	0.01	.228E+29	28.358
69	3C228	0.85	0.03	.684E+28	27.835	0.85	0.03	.684E+28	27.835
70	3C231	0.54	0.03	.426E+23	22.629	0.54	0.03	.426E+23	22.629
71	3C234	0.97	0.02	.969E+27	26.986	1.00	0.03	.948E+27	26.977
72	3C239	1.17	0.02	.0	0.0	1.17	0.02	.0	0.0
73	3C241	1.14	0.06	.0	0.0	1.14	0.06	.0	0.0
74	3C244.1	0.98	0.03	.454E+28	27.657	0.98	0.03	.454E+28	27.657
75	3C245	0.68	0.0	.274E+29	28.438	0.68	0.0	.274E+29	28.438
76	3C247	0.85	0.02	.347E+28	27.540	0.85	0.02	.347E+28	27.540
77	3C249.1	0.82	0.05	.122E+28	27.088	0.90	0.03	.119E+28	27.076
78	3C250	1.21	0.07	.782E+28	27.893	1.21	0.07	.782E+28	27.893
79	3C252	1.14	0.04	.712E+28	27.852	1.14	0.04	.712E+28	27.852
80	3C254	1.04	0.06	.144E+29	28.158	1.04	0.06	.144E+29	28.158
81	3C263	0.85	0.01	.908E+28	27.958	0.91	0.01	.897E+28	27.953
82	3C263.1	1.04	0.03	.383E+28	27.584	1.04	0.03	.383E+28	27.584
83	3C264	0.84	0.01	.112E+26	25.050	0.91	0.01	.108E+26	25.031
84	3C265	1.10	0.05	.169E+29	28.227	1.10	0.05	.169E+29	28.227
85	3C266	1.18	0.08	.271E+29	28.434	1.18	0.08	.271E+29	28.434
86	3C267	0.91	0.07	.0	0.0	0.91	0.07	.0	0.0
87	3C268.1	0.72	0.02	.0	0.0	0.72	0.02	.0	0.0
88	3C268.3	0.86	0.04	.289E+28	27.461	0.86	0.04	.289E+28	27.461
89	3C268.4	0.96	0.02	.486E+29	28.687	0.99	0.03	.500E+29	28.699
90	3C270.1	0.93	0.02	.784E+29	28.894	1.08	0.02	.806E+29	28.906
91	3C272	1.05	0.11	.0	0.0	1.05	0.11	.0	0.0
92	3C272.1	0.62	0.03	.268E+24	23.429	0.63	0.03	.263E+24	23.420
93	3C274	0.84	0.02	.176E+26	25.246	0.87	0.02	.173E+26	25.238
94	3C274.1	1.00	0.02	.313E+28	27.495	1.00	0.02	.313E+28	27.495
95	3C275.1	0.92	0.02	.622E+28	27.794	1.02	0.02	.605E+28	27.782
96	3C277.2	0.91	0.05	.950E+28	27.978	0.91	0.05	.950E+28	27.978
97	3C277.3	0.65	0.03	.981E+26	25.992	0.66	0.03	.974E+26	25.989
98	3C280	0.86	0.05	.605E+28	27.782	0.86	0.05	.605E+28	27.782
99	3C280.1	1.08	0.06	.623E+29	28.795	1.16	0.05	.642E+29	28.807
100	3C284	0.82	0.02	.551E+27	26.741	0.82	0.02	.551E+27	26.741
101	3C285	0.75	0.02	.587E+26	25.768	0.75	0.02	.584E+26	25.766
102	3C286	0.51	0.02	.675E+29	28.829	0.51	0.02	.675E+29	28.829
103	3C287	0.58	0.01	.567E+29	28.754	0.58	0.01	.567E+29	28.754
104	3C288	0.97	0.01	.111E+28	27.046	0.98	0.01	.111E+28	27.043
105	3C289	1.02	0.04	.0	0.0	1.02	0.04	.0	0.0
106	3C293	0.71	0.01	.414E+26	25.617	0.71	0.01	.414E+26	25.617
107	3C294	1.17	0.09	.0	0.0	1.17	0.09	.0	0.0
108	3C295	0.93	0.03	.309E+29	28.489	0.93	0.03	.309E+29	28.489
109	3C296	0.62	0.06	.104E+26	25.016	0.63	0.06	.102E+26	25.009
110	3C299	0.91	0.04	.241E+28	27.383	0.91	0.04	.241E+28	27.383
111	3C300	0.94	0.0	.143E+28	27.157	0.94	0.0	.144E+28	27.157
112	3C303	0.78	0.03	.254E+27	26.405	0.87	0.04	.240E+27	26.380
113	3C303.1	1.11	0.19	.767E+27	26.885	1.11	0.19	.767E+27	26.885
114	3C305	0.90	0.03	.234E+26	25.369	0.90	0.03	.234E+26	25.369
115	3C305.1	0.94	0.08	.228E+28	27.358	0.94	0.08	.228E+28	27.358
116	3C309.1	0.60	0.01	.470E+29	28.672	0.60	0.01	.470E+29	28.672
117	3C310	1.28	0.05	.107E+27	26.031	1.30	0.05	.106E+27	26.024
118	3C314.1	1.15	0.05	.136E+27	26.133	1.15	0.05	.136E+27	26.133

3: Spectral indices and luminosities.

		(1)	(2)	(3)	(4)	(5)	(6)	(7)	(8)
9	3C315	0.88	0.04	.228E+27	26.359	0.95	0.05	.214E+27	26.330
0	3C318	0.95	0.02	.115E+29	28.060	0.95	0.02	.115E+29	28.060
1	3C319	1.03	0.02	.479E+27	26.681	1.03	0.02	.479E+27	26.681
2	3C321	0.86	0.01	.154E+27	26.187	0.87	0.01	.153E+27	26.183
3	3C322	1.09	0.05	.0	0.0	1.09	0.05	.0	0.0
4	3C324	1.06	0.03	.136E+29	28.135	1.06	0.03	.136E+29	28.135
5	3C325	1.02	0.08	.0	0.0	1.02	0.08	.0	0.0
6	3C330	0.84	0.03	.136E+29	28.133	0.84	0.03	.136E+29	28.133
7	3C334	0.90	0.14	.446E+28	27.649	0.98	0.16	.432E+28	27.635
8	3C336	0.95	0.07	.210E+29	28.322	0.95	0.07	.210E+29	28.322
9	3C337	0.93	0.0	.942E+28	27.974	0.93	0.0	.942E+28	27.974
0	3C338	1.55	0.03	.146E+26	25.165	1.68	0.05	.138E+26	25.140
1	3C340	0.92	0.07	.135E+28	27.129	0.92	0.07	.135E+28	27.129
2	3C341	0.96	0.05	.275E+28	27.439	0.96	0.05	.275E+28	27.439
3	3C343	0.91	0.06	.469E+29	28.671	0.91	0.06	.469E+29	28.671
4	3C343.1	1.03	0.06	.225E+29	28.352	1.03	0.06	.225E+29	28.352
5	3C345	0.17	0.02	.118E+29	28.072	0.17	0.02	.118E+29	28.072
6	3C346	0.69	0.02	.474E+27	26.675	0.69	0.02	.474E+27	26.675
7	3C349	0.80	0.05	.715E+27	26.855	0.81	0.05	.716E+27	26.855
8	3C351	0.78	0.06	.281E+28	27.449	0.78	0.05	.278E+28	27.445
9	3C352	1.05	0.05	.112E+29	28.048	1.05	0.05	.112E+29	28.048
0	3C356	1.10	0.03	.0	0.0	1.10	0.03	.0	0.0
1	3C368	1.34	0.03	.128E+29	28.109	1.34	0.03	.128E+29	28.109
2	3C380	0.58	0.04	.436E+29	28.640	0.58	0.04	.436E+29	28.640
3	3C381	0.78	0.07	.486E+27	26.687	0.78	0.07	.486E+27	26.687
4	3C382	0.76	0.0	.877E+26	25.943	0.81	0.01	.833E+26	25.921
5	3C386	0.76	0.03	.903E+25	24.956	0.76	0.03	.903E+25	24.956
6	3C388	0.90	0.01	.221E+27	26.344	0.92	0.02	.219E+27	26.339
7	3C390.3	0.72	0.04	.159E+27	26.201	0.77	0.02	.155E+27	26.190
8	3C401	0.92	0.05	.101E+28	27.006	0.94	0.05	.100E+28	27.000
9	3C427.1	1.06	0.03	.135E+29	28.129	1.06	0.03	.135E+29	28.129
0	3C432	1.07	0.05	.817E+29	28.912	1.07	0.05	.817E+29	28.912
1	3C433	0.91	0.0	.573E+27	26.758	0.91	0.0	.573E+27	26.758
2	3C436	0.93	0.03	.814E+27	26.911	0.94	0.03	.811E+27	26.909
3	3C437	0.93	0.01	.0	0.0	0.93	0.01	.0	0.0
4	3C438	1.14	0.02	.339E+28	27.530	1.14	0.02	.339E+28	27.530
5	3C441	0.80	0.01	.121E+29	28.084	0.80	0.01	.121E+29	28.084
6	3C442A	0.59	0.0	.104E+26	25.018	0.59	0.0	.104E+26	25.018
7	3C449	0.66	0.07	.468E+25	24.670	0.67	0.08	.463E+25	24.665
8	3C452	0.93	0.02	.321E+27	26.507	0.95	0.02	.318E+27	26.503
9	3C454	0.79	0.02	.813E+29	28.910	0.79	0.02	.813E+29	28.910
0	3C454.3	-0.14	0.25	.405E+29	28.608	-0.14	0.25	.405E+29	28.608
1	3C455	0.94	0.03	.576E+28	27.761	0.94	0.03	.576E+28	27.761
2	3C460	1.08	0.08	.621E+27	26.793	1.07	0.08	.608E+27	26.784
3	3C465	0.87	0.04	.297E+26	25.473	0.93	0.04	.286E+26	25.456
4	3C469.1	1.06	0.06	.0	0.0	1.06	0.06	.0	0.0
5	3C470	1.02	0.03	.0	0.0	1.02	0.03	.0	0.0